

We are IntechOpen, the world's leading publisher of Open Access books Built by scientists, for scientists

6,300

Open access books available

171,000

International authors and editors

190M

Downloads

Our authors are among the

154

Countries delivered to

TOP 1%

most cited scientists

12.2%

Contributors from top 500 universities



WEB OF SCIENCE™

Selection of our books indexed in the Book Citation Index
in Web of Science™ Core Collection (BKCI)

Interested in publishing with us?
Contact book.department@intechopen.com

Numbers displayed above are based on latest data collected.
For more information visit www.intechopen.com



AWJ machining has many advantages over other nonconventional techniques [4]:

- It can cut a wide range of materials including titanium, stainless steel, aerospace alloys, glass, plastics, ceramics, and so on.
- It can cut net-shaped parts and near net-shaped parts.
- There are no heat-affected areas; thus, no structural changes in work materials occur because no heat is generated in the cutting process.
- It is particularly environmentally friendly as it does not cause any cutting dust or chemical air pollutants.
- Only one nozzle is needed to machine various types of work materials and workpiece shapes.
- AWJ machining can be easily automated, and therefore it can be run with unmanned shifts.

2. Abrasive waterjet system

Figure 1 shows a typical AWJ entrainment system. There are four main parts in the system. They are the water preparation system, the pressure generation system, the jet former, and

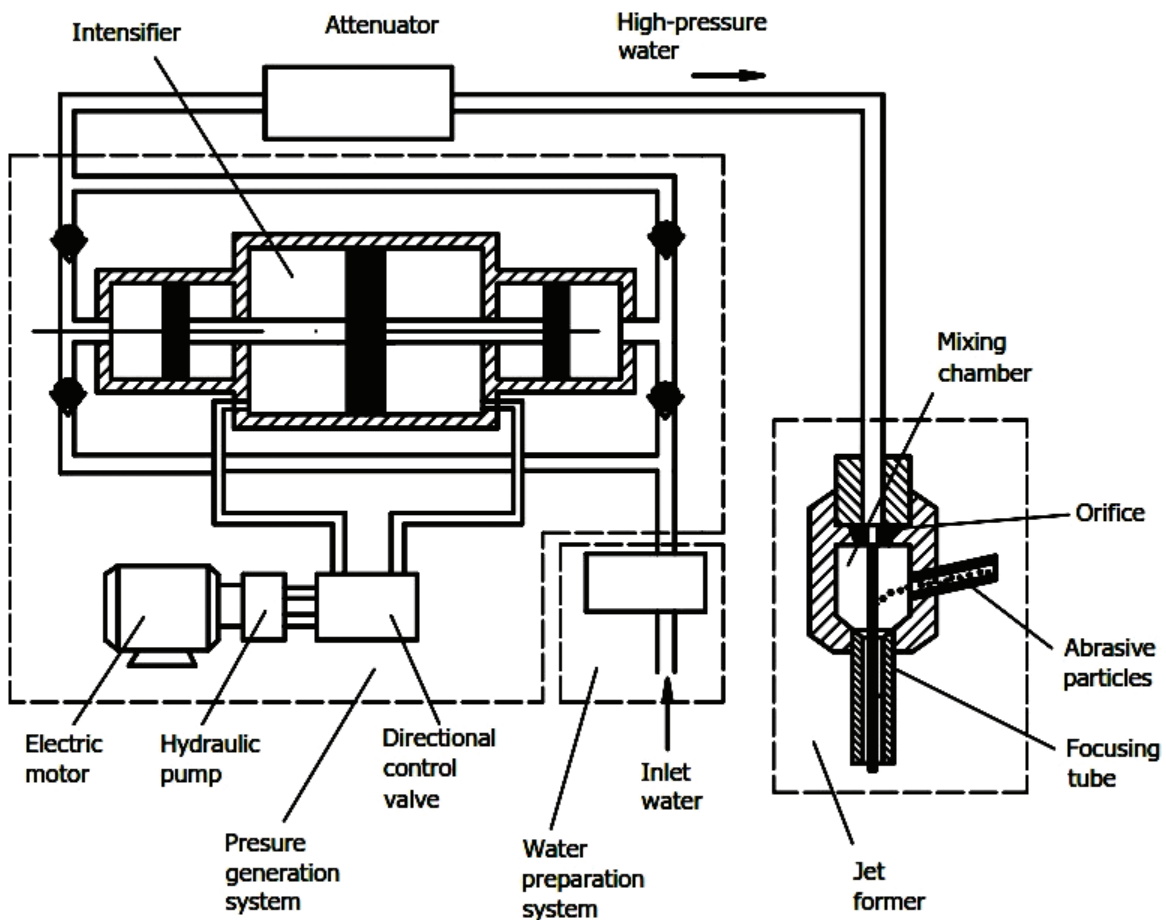


Figure 1. Schema of an AWJ machining system [4].

the abrasive supply system. An abrasive waterjet entrainment system mixes abrasives with the waterjet in a mixing chamber. The abrasive particles are accelerated by the high-velocity water stream and then leave the focusing tube (or the nozzle) with the stream. The high-velocity beam of water and abrasives is used for cutting harder materials such as stainless steel, glass, ceramics, titanium alloys, composite materials, and so forth.

3. Challenges in abrasive waterjet technology

Although AWJ machining has a number of advantages as described in Section 1, a considerable disadvantage of this technology is its relatively high cutting cost. Therefore, the reduction of the machining cost is a significant challenge in this technology.

In order to reduce AWJ machining cost, there are two possible solutions including optimization of the machining process and abrasive recycling. For the first solution, until now, there have been many studies in optimizing AWJ's factors that include jet parameters (e.g., water pressure, orifice diameter, focusing tube diameter, focusing tube length, abrasive mass flow rate, abrasive size, abrasive shape, and abrasive type) and cutting parameters (e.g., the stand-off distance, the work material, and the feed speed).

For optimum selection of focusing tube and orifice diameters, H. Blickwedel [5] introduced an optimum ratio between the focusing tube diameter and the orifice diameter. Zeng and Munoz [6] also reported the optimum combination of focusing tube/orifice for the highest AWJ cutting performance. The optimum focusing tube length for maximum depth of cut was proposed by Blickwedel [5]. Hashish [7] noted that the depth of cut and the kerf width both depend on the length of the focusing tube. In addition, a new way for using the focusing tube in order to get the minimum cutting cost was proposed [8].

Numerous studies have been carried out on optimum abrasive mass flow rate. The optimum abrasive mass flow rate for the maximum cutting performance (or for the maximum depth of cut) depends on many parameters including the water pressure [9–11], the orifice diameter [9, 11], the focusing tube diameter [9, 10, 12], and the focusing tube length [10].

The effects of other parameters on the depth of cut have also been investigated. Those are the abrasive particle sizes [13] and the standoff distance [5, 14]. For getting the minimum cutting time, the minimum cutting cost, and the maximum profit rate, Vu Ngoc Pi [4] carried out a study on AWJ optimization. In the study, models for determination of the optimum abrasive mass flow rate and the optimum nozzle exchanged diameter were proposed.

The other solution to enhance AWJ cutting cost is abrasive recycling. So far, there were several studies on this area. Labus et al. [15] presented a fundamental research on the influence of the process parameters on the particle size distribution after the mixing process and after the cutting process. The authors found that the water pressure from 0 to 205 MPa had more influences on the fraction of abrasive particles than the pressure from 274 to 342 MPa. Furthermore, the geometry of the mixing chamber affected the distribution of abrasive particle size. It was also noted that the particle fraction was not connected to the length of the mixing tube.

Louis et al. [16] explored the influences of cutting parameters on the fragmentation of abrasive particles after penetration to the workpiece. It was mentioned that after the workpiece, the average size of particles was smaller than that after the focusing tube. In addition, the authors found that the particle fragmentation depended on the workpiece materials. For instance, the particle size after cutting stainless steel was smaller than after cutting aluminum. Furthermore, the fragmentation after workpiece of different abrasive materials was inspected. The authors reported that olivine produced a slightly smaller average particle size than garnet [16].

For evaluation of the fragmentation of abrasive particles, Ohlsen [13] introduced a “disintegration number” in a systematic study on the recycling of Barton garnet. In the study, the effects of different process parameters on the magnitude of the disintegration number were investigated, such as the water pressure, the abrasive mass flow rate, the abrasive particle diameter, the focusing tube diameter, and the focusing tube length.

Another study on the abrasive recycling was performed for a local garnet from India [17]. In this study, the reusability of the garnet was investigated with four recycling cycles. It was found that the recycling capacity (or the reusability) of the first, the second, the third, and the fourth recycling was 81, 49, 26, and 15%, respectively. In addition, the influences of recycled abrasives on the cutting performance and the cutting quality were explored.

In order to increase and preserve the cutting performance of recycled abrasives, new abrasives are added into recycled abrasives. This process is called recharging of abrasives. Kantha Babu and Krishnaiah Chetty [18] announced the results of an abrasive recharging study. It was reported that an increase of the added new abrasives up to 40% led to a significant increase of the depth of cut and a slight increase thereafter. Subsequently, in order to get the maximum depth of cut, the recharging at 40% of the recycled abrasive mass was recommended. Besides, the percentage of added abrasives as well as the cutting performance and the cutting quality of recharged abrasives was examined.

Vu Ngoc Pi et al. [19] carried out a study on the recycling and recharging of GMA abrasive. In the research, the reusability of GMA abrasive after the first cut and second cut was explored. In addition, the reusability of the recharged abrasives was explored. Furthermore, the cutting performance and the cutting quality of both recycled abrasive and recharged abrasive were investigated. The optimal particle sizes for the recycling and the recharging of GMA garnet were also proposed.

The cutting performance and the economics when using recycled and recharged GMA abrasives were evaluated in another study of Vu Ngoc Pi [4]. It was concluded that the cutting performance when cutting with recycled and recharged abrasives is higher than that when cutting with the new abrasive (about 17% when cutting with recycled abrasives and 10% when cutting with recharged abrasive). Also, cutting with those abrasives can reduce the total cutting cost and increase the profit rate significantly [4].

4. Recycling and recharging of supreme garnet

In this chapter, the recycling and recharging of Supreme garnet are investigated. In the study, the reusability of the garnet, the cutting performance, and the cutting quality of the recycled

and recharged abrasive are explored. Also, the optimum particle size for getting the maximum cutting performance for both recycling and recharging of Supreme garnet is determined.

4.1. Reusability of supreme garnet

4.1.1. Experimental setup

Figure 2 describes the experimental setup for determination of the reusability of the garnet. The cutting system consists of a M23120B Flow Waterjet machine and a cutting head with a focusing tube diameter of 1.02 mm and an orifice diameter of 0.33 mm. The workpiece material is SUS 304, the abrasive is IMC garnet #80, and the cutting regime is as follows: the water pressure of 350 MPa, the abrasive mass flow rate of 300 g/min, and the feed speed of 90 mm/min. For abrasive sieving, a sieve shaker and 11 sieves (ISO3310-1) are used. The nominal aperture sizes of the sieves are 63, 75, 90, 106, 125, 150, 180, 212, 250, 300, and 355 μm , respectively. To investigate the reusability of the first recycling, the abrasives after cutting are collected, washed, dried, chips separated, sieved, and sorted.

In AWJ cutting process, the fragmentation (or the breaking) of abrasive particles occurs in two stages [4]: during mixing process (due to the interactions between particles and the mixing chamber walls and focusing tube and between particles with each other) and during the cutting process (due to the interactions between particles with the workpiece and particles

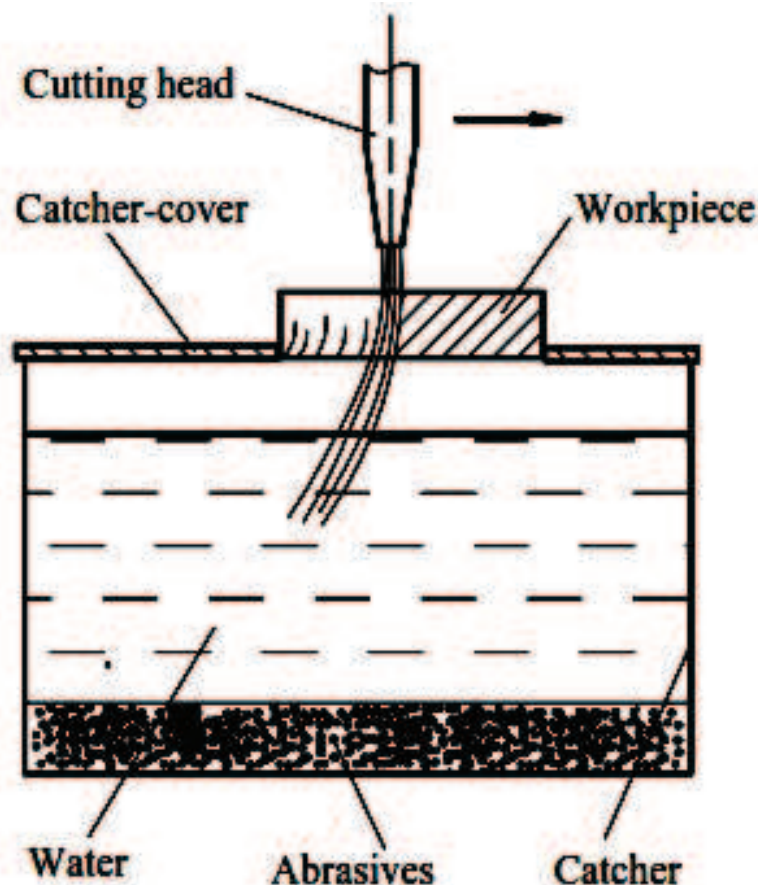


Figure 2. Experimental setup for collecting abrasives [4].

with each other). Therefore, studying the abrasive recycling needs an understanding of the fragmentation of abrasive particle in both above stages.

The experiment for investigating the abrasive fragmentation after focusing tube is the same as in **Figure 2**. However, in this experiment, no workpiece was used. After coming into water tank, the abrasives were collected and dried. After that, they were sieved and sorted into different sizes. The experiment was performed with four recycled abrasive samples (with particle sizes larger than 90, 106, 125, and 150 μm) and a new Supreme garnet sample.

4.1.2. Results and discussions

Table 1 presents the reusability of the garnet after the first cut. Similar to GMA garnet [19], the reusability of Supreme garnet decreases with the increase of the recycled particle size. It is noted that Supreme garnet can be reused better than GMA garnet. As it can be seen in **Table 1**, the reusability of Supreme garnet (with particles larger 90 μm) is 58.86%, while it is 53.64% with GMA garnet [19].

Figure 3 describes the relation between retained particle mass and the particle size after the mixing process. It is found that, with all abrasive samples, the retained particle mass with the size larger than 150 μm is nearly the same. Nevertheless, with the size smaller than 150 μm , the retained particle mass is significantly different from each other. Also, the retained particle mass of all recycled abrasive samples with the size smaller 150 μm is higher than that of the new ones.

Sieve size (μm)	>90	>106	>125	>150	>180	>212	>250
Reusability (%)	58.86	53.4	47.0	38.7	27.4	16.4	4.6

Table 1. Reusability after the first cut.

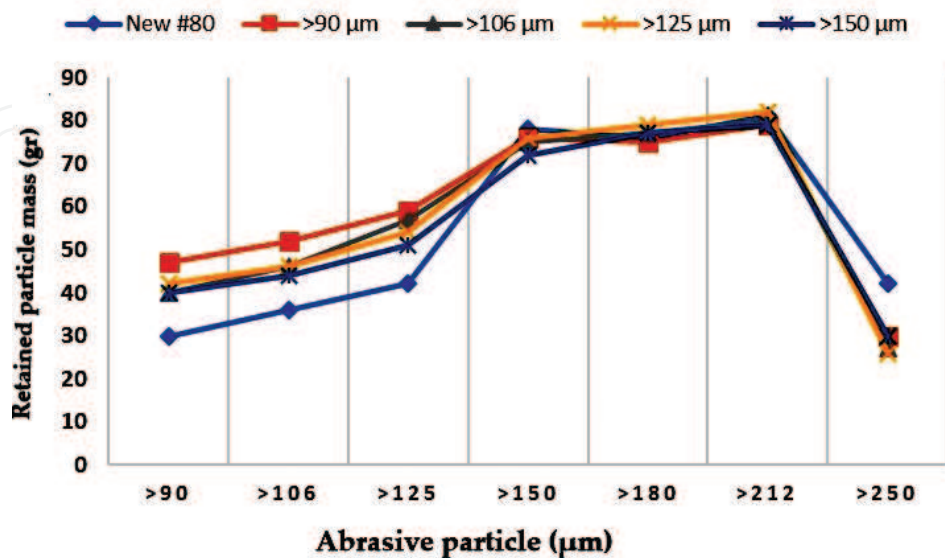


Figure 3. Retained particle mass versus recycled particle size after mixing process.

4.2. Cutting performance and cutting quality of recycled abrasives

4.2.1. Experimental setup

Figure 4 shows the experiment setup for comparison of the cutting performance (or the maximum depth of cut) between the new and recycled abrasives. The workpiece in this experiment is described on **Figure 5**, and its material is SUS304. In the experiment, four samples of recycled abrasives (with particles larger than 90, 106, 125, and 150 μm) and a sample of new Supreme garnet #80 are used for the test. Each abrasive sample is tested with five cuts and with two replications. The AWJ cutting parameters used in the experiment include the water pressure of 350 MPa, the abrasive mass flow rate of 540 g/min, the orifice diameter of 0.33 mm, the nozzle diameter of 1.02 mm, and the feed speed of 100, 125, 150, 175, and 200 mm/min.

In order to investigate the effects of the recycled abrasives on the surface roughness, four recycled abrasive samples (as mentioned above) and a new Supreme garnet #80 are tested (with two replications) with the following cutting regime: the workpiece material of SUS304,



Figure 4. Experimental setup for determination of maximum depth of cut.

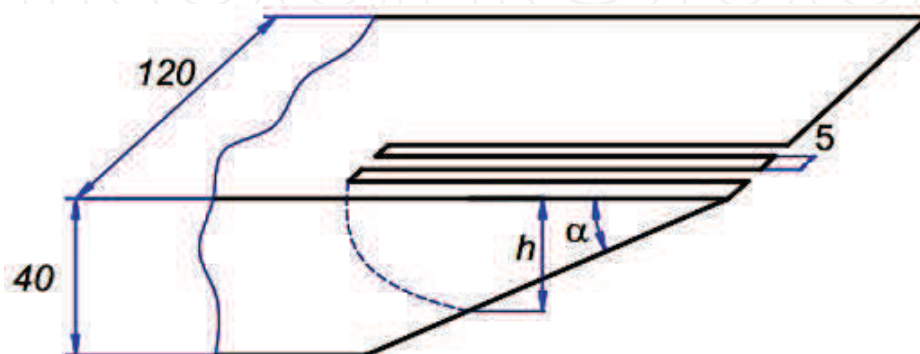


Figure 5. Workpiece used in experiment for determination of maximum depth of cut [20].

the water pressure of 350 MPa, the abrasive mass flow rate of 540 g/min, the feed speed of 125, 150, 175 and 200 mm/min, the focusing tube diameter of 1.02 mm, and the orifice diameter of 0.33 mm.

4.2.2. Results and discussions

Figure 6 shows the cutting performance of the recycled abrasives. It is noticed that the cutting performance of all recycled samples is slightly higher than that of the new Supreme garnet #80. This can be explained that after mixing process, with the new sample, the mass of retained particles with the size $<150\ \mu\text{m}$ is less than that of all recycled samples (**Figure 3**). Consequently, the number of recycled particles involved in the cutting process is higher than that of the new sample. Hence, the removed workpiece volume and therefore the cutting performance grow. It is also found that there is an optimum value of the recycled abrasive size (particle size larger than $90\ \mu\text{m}$) with which the cutting performance is maximum.

To evaluate the influence of recycled abrasives on the cutting quality, the surface roughness (R_a) is measured (**Figure 7**) at six values of the depth from 5 to 30 mm. **Figure 8** describes the average of the surface roughness of three replications of tests. It is detected that the surface roughness of the recycled abrasive is slightly lower than that of the new. The reason is that although the recycled particles are smaller than the new ones, they are sharper. As a result, the influences of the recycled abrasive size and shape on the surface roughness can be considered equivalent.

4.3. Cutting performance and cutting quality of recharged abrasives

4.3.1. Experimental setup

In order to find the optimum particle size of recharged abrasives, four samples of the first recycled abrasives (with the particle size larger than 90, 106, 125, and $150\ \mu\text{m}$) are recharged

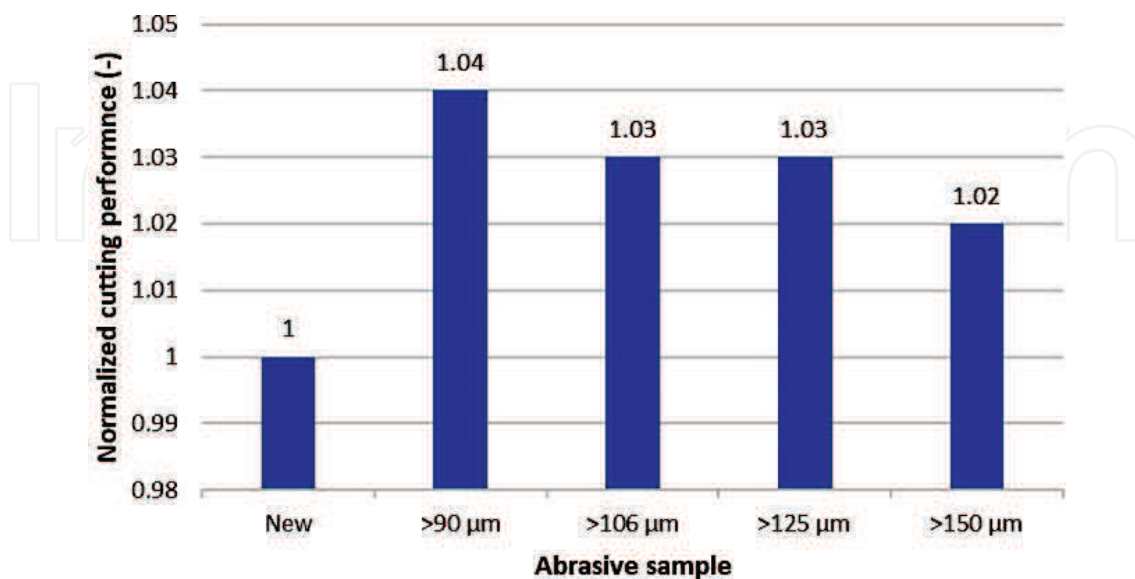


Figure 6. Cutting performance of recycled abrasives.



Figure 7. Measurement of surface roughness.

with the new abrasive (Supreme garnet #80) for getting the same amount of abrasives (100%) (Table 2). To investigate the cutting performances of these recharged samples, experiments with the same setup as that for the cutting performance of the recycled abrasives (Figure 4) are carried out.

To investigate the effects of the recharged abrasives on the cutting performance and cutting quality, four recharged abrasive samples (as mentioned above) and a new Supreme garnet #80 are tested (with two replications). The cutting regime of these experiments consists of the

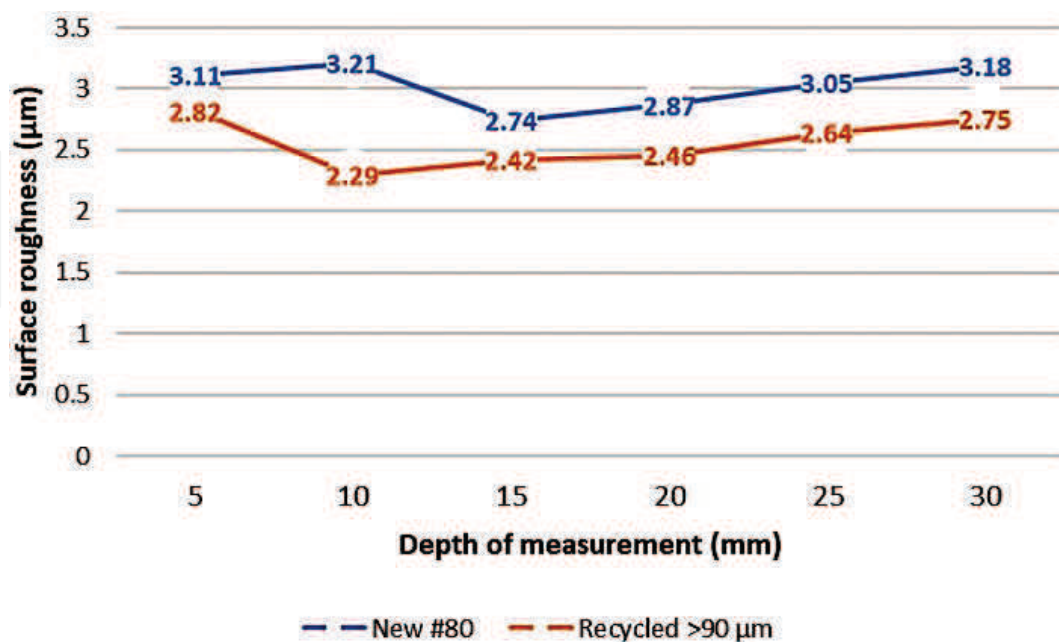


Figure 8. Surface roughness when cutting with recycled abrasives.

Sample	Sieve nominal aperture size (μm)	Reusability (%)	Recharged abrasive (%)
1	150	58.8	41.2
2	125	53.4	46.6
3	106	47.0	53.0
4	90	38.7	61.3

Table 2. Recharging abrasives.

workpiece material of SUS304; the water pressure of 350 MPa; the abrasive mass flow rate of 540 g/min; the feed speed of 125, 150, 175, and 200 mm/min; the focusing tube diameter of 1.02 mm; and the orifice diameter of 0.33 mm.

4.3.2. Results and discussions

Figure 9 presents the cutting performance of the recharged abrasives. It is observed that the cutting performance of all recharged samples is higher than that of the new Supreme garnet #80. The reason of that is the same with recycled samples (see Section 4.2.2): with all recharged samples, the mass of retained particles with the size smaller than 150 μm is higher than that of the new (see **Figure 10**). Hence, the particle in the recharged samples and then the particle number taking part in the cutting process increase. Consequently, the volume of removed work material growth and therefore the cutting performance increase. It is also detected that the particle size larger than 90 μm is the optimum value with which the cutting performance is maximum.

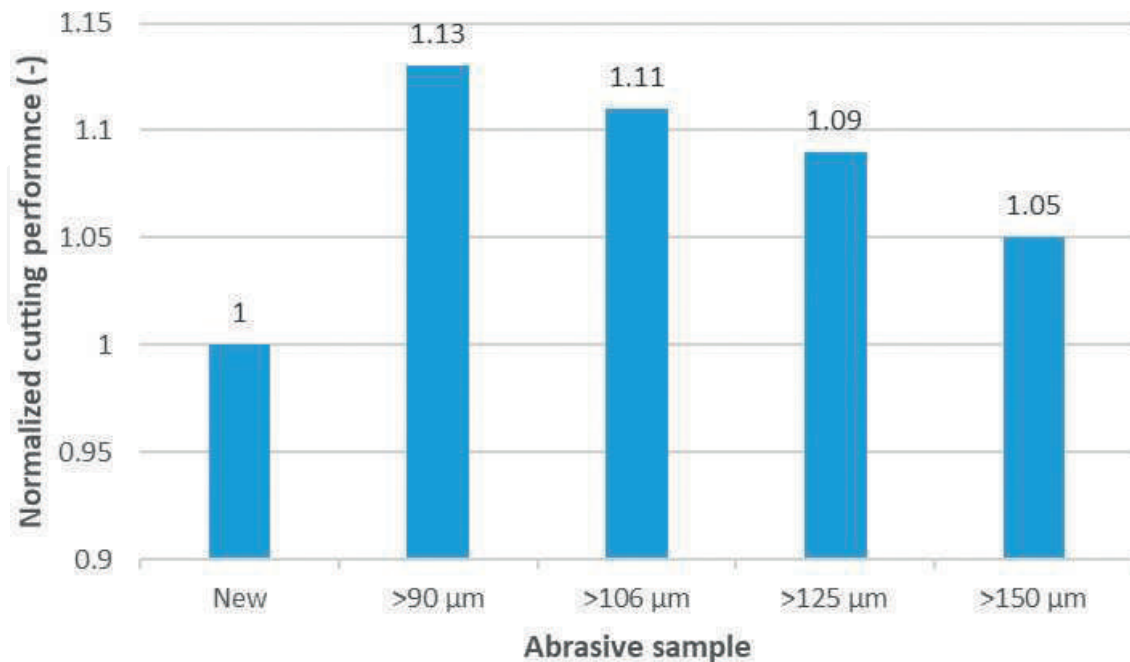


Figure 9. Cutting performance of recharged abrasives.

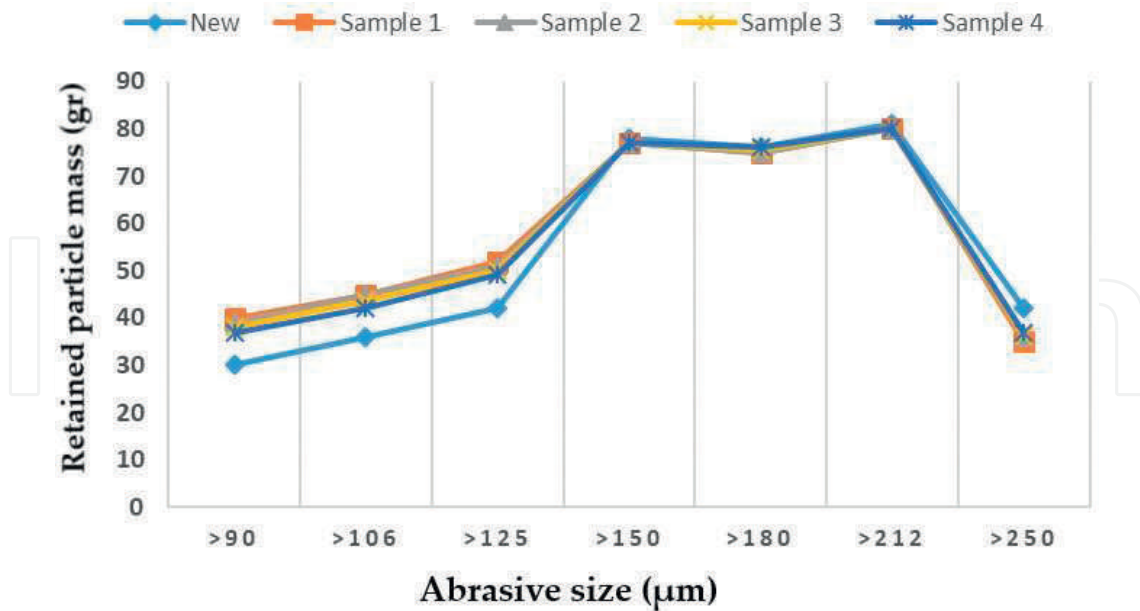


Figure 10. Retained particle mass versus recharged particle size after mixing process.

In order to evaluate the effect of recharged abrasives on the cutting quality, the surface roughness (R_a) is measured at six values of the depth from 5 to 30 mm. **Figure 11** shows the average of the surface roughness of three replications of tests. It is found that the surface roughness when cutting with recharged abrasive is slightly lower than that when cutting with new Supreme garnet #80. As it was explained above (in Section 4.2.2), in spite of the fact that the recharged particles are smaller than the new ones, they are sharper. Hence, the effects of the recharged abrasive size and shape on the surface roughness are considered equivalent.

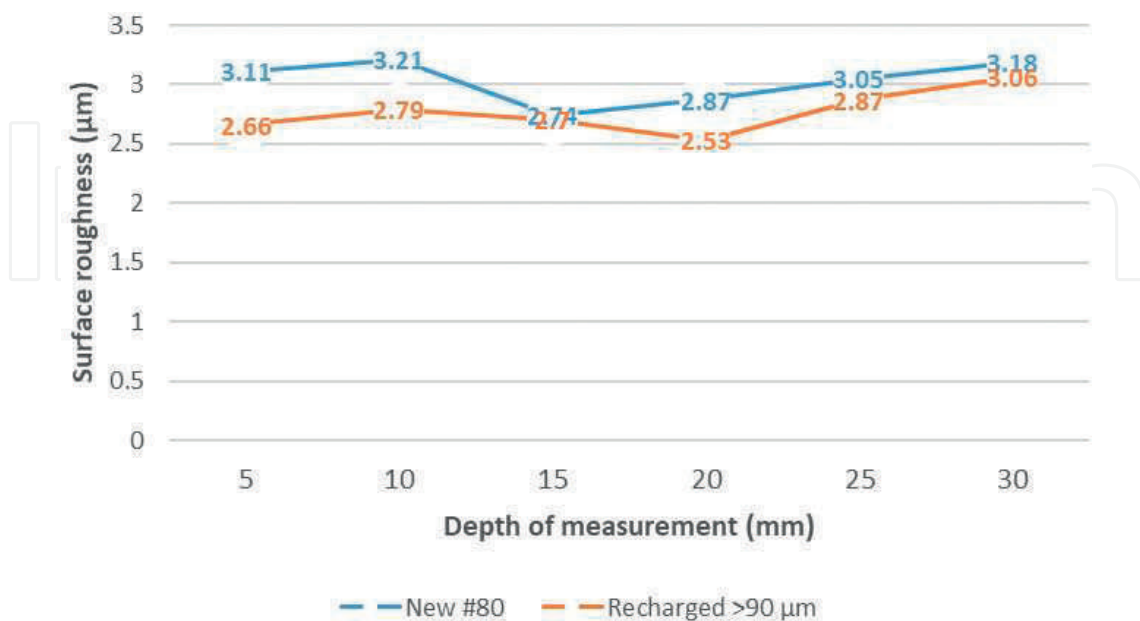


Figure 11. Surface roughness when cutting with recharged abrasives.

5. Conclusions

In this chapter, the investigation of recycling and recharging of Supreme garnet, including the reusability of the abrasive, the cutting performance, and the cutting quality of the recycled and recharged abrasives, has been carried out. Several conclusions can be obtained from the investigation as follows:

- The reusability of Supreme garnet is higher than that of GMA garnet. For example, with the particle size of $>90\ \mu\text{m}$, the reusability of Supreme garnet is 58.86%, while it is only 53.64% for GMA garnet.
- The cutting performance of recycled and recharged Supreme abrasives is slightly higher than that of the new Supreme garnet #80.
- The optimum particle size for the cutting performance is larger than $90\ \mu\text{m}$ for both the recycling and the recharging.

Author details

Vu Ngoc Pi^{1*} and Tran Quoc Hung²

*Address all correspondence to: vungocpi@tnut.edu.vn

1 Thai Nguyen University of Technology, Thai Nguyen City, Vietnam

2 Hanoi University of Industry, Ha Noi City, Vietnam

References

- [1] Summers DA. Waterjet Technology. Chapman & Hall; UK. 1995
- [2] Tikhomirov RA, Babanin VF, Petukhov EN, Starikov ID, Kovaleb VA. High-Pressure Jetcutting. ASME Press; USA. 1992
- [3] Hashish M, Kirby M, Pao Y-H. Method and apparatus for forming a high velocity liquid abrasive jet. United States Patent No. 4,648,215. Filed October 7, 1985, Issued March 10, 1987
- [4] Vu Ngoc Pi. Performance enhancement of abrasive waterjet cutting [PhD thesis]. Delft University of Technology; 2008
- [5] Blickwedel H. Erzeugung und Wirkung von Hochdruck-Abrasivstrahlen. VDI Fortschritt – Berichte. Reihe 2, Nr. 206, 1990
- [6] Zeng J, Munoz J. Optimization of abrasive waterjet cutting- the abrasive issues. SME Technical Paper. 1994:MR94-M247

- [7] Hashish M. Optimization factors in abrasive-waterjet machining. *Journal of Engineering for Industry*. 1991;**113**:29-37
- [8] Vu Ngoc Pi, Hoogstrate MA, Karpuschewski B. Cost optimization and a new and effective way of using AWJ nozzles. In: 5th International Conference of PhD Students; Hungary. 2005. pp. 153-165
- [9] Chalmers EJ. Effect of parameter selection on abrasive waterjet performance. In: 6th American Water Jet Conference; August 24-27, 1991; Houston, Texas. pp. 345-354
- [10] Guo NS. Schneidprozeß und Schnittqualität beim Wasserabrasivstrahlschneiden, VDI-Fortschritt-Berichte, Reihe 2, Nr. 328. 1994
- [11] Guo NS, Louis H, Meier G, Ohlsen J. Abrasive water jet cutting—Methods to calculate cutting performance and cutting efficiency. In: Rakowski, editor. *Geomechanics 93*. Balkema, Rotterdam; 1994. pp. 291-299
- [12] Hoogstrate AM, Susuzlu T, Karpuschewski B. Abrasive waterjet cutting beyond 400 MPa. In: 2005 WJTA American Waterjet Conference; August 21-23, 2005; Houston, Texas
- [13] Ohlsen J. Recycling von Feststoffen beim Wasserabrasivstrahlverfahren. VDI Fortschritt-Berichte, Reihe 15, Nr. 175; 1997
- [14] Barton RE. A safe method of cutting steel and rock. In: 6th International Symposium on Jet Cutting Technology; BHRA Fluid Engineering, Cranfield; 1982. pp. 503-518
- [15] Labus TJ, Neusen KF, Alberts DG, Gores TJ. Factors influencing the particle size distribution in an abrasive waterjet. *Journal of Engineering for Industry*. 1991;**113**:402-411
- [16] Louis H, Meier G, Ohlsen J. Analysis of the process output in abrasive water jet cutting. In: 8th American Water Jet Conference; August 26-29, 1995; Houston, Texas. pp. 137-151
- [17] Kantha Babu M, Krishnaiah Chetty OV. A study on recycling of abrasives in abrasive water jet machining. *Wear*. 2003;**254**:763-773
- [18] Kantha Babu M, Krishnaiah Chetty OV. Studies on recharging of abrasives in abrasive water jet machining. *International Journal of Advanced Manufacturing Technology*. 2002;**19**:697-703
- [19] Ngoc Pi V, Gonfiotti P, Hoogstrate AM, Karpuschewski B. A study on abrasive recycling and recharging in Abrasive Waterjet (AWJ) Machining. *International Journal of Machining and Machinability*. 2009;**6**(3/4). DOI: 10.1504/IJMMM.2009.027325
- [20] Pi VN, Chau HV, Hung TQ. A study on recycling of supreme garnet in abrasive waterjet machining. *Applied Mechanics and Materials*. 2013;**248**:499-503. DOI: 10.4028/www.scientific.net/AMM.248.499

We are IntechOpen, the world's leading publisher of Open Access books Built by scientists, for scientists

6,300

Open access books available

171,000

International authors and editors

190M

Downloads

Our authors are among the

154

Countries delivered to

TOP 1%

most cited scientists

12.2%

Contributors from top 500 universities



WEB OF SCIENCE™

Selection of our books indexed in the Book Citation Index
in Web of Science™ Core Collection (BKCI)

Interested in publishing with us?
Contact book.department@intechopen.com

Numbers displayed above are based on latest data collected.
For more information visit www.intechopen.com



Nanostructural Deformation in Brittle-Ductile Compounds and Its Application in Fabricating Ductile Nanoparticles

Babak Alinejad and Yazdan Zare

Additional information is available at the end of the chapter

<http://dx.doi.org/10.5772/intechopen.76787>

Abstract

The ball-milling process involves both fracturing and welding of particles. Particles of ductile materials are very likely to attach to each other when entrapped between balls. Therefore, conventional milling methods fail to grind ductile materials into nanoparticles. However, using brittle particles together with the starting materials, one can fracture and highly activate ductile particles through planetary ball milling. During the milling process, brittle particles are easily fractured down, and their sharp edges chop the particles of the ductile materials incessantly into pieces until both ductile and brittle particles are nano-sized (a process which is unlikely, if not impossible, to accomplish by ball milling of ductile materials alone). In this chapter, the effects of ball milling of ductile materials (e.g., graphite, aluminum, and zinc) together with a brittle material (here, NaCl), for preparation of metal nanoparticles or metal oxide nanoparticles are investigated. A theoretical explanation of the mechanism is also presented based on the facts and practical measurements.

Keywords: ball milling, brittle, ductile, nanoparticle, nanochopper, graphene

1. Introduction

In every branch of material engineering, it happens very frequently that a bulk material is ground into very fine particles. Therefore, material engineers are quite acquainted with grinding process. Having basic principles in common, grinding methods may be slightly different depending on the characteristics of the material that is about to be ground, ultimate size of particles after grinding, energy- and time-consumption condensations (which may also be referred to as economy of the process), etc.

One of the most routine methods for grinding is planetary ball milling in which a given material is loaded in a jar that is partially filled with balls made of a harder material (e.g., stainless steel and zirconia). The jar is then sealed and rotates multi-directionally by means of electro-motors. The bulk material is gradually ground as the balls exert large enough compressive and shear stresses on it to fracture it into fine particles. For most of the materials, the longer the ball-milling duration, the smaller the particle size. However, as we will see soon in this chapter, this is not always the case. Particles of ductile materials rejoin together to form larger particles when they are shoved into each other by the balls (this phenomenon is referred to as *cold-welding*). Hence, the ball milling does not necessarily lead to size reduction of the particles.

Introduced in this chapter is a new, simple method for ball milling of ductile materials (the method has already been examined for some ductile materials). When the materials to be ground are all ductile, then a brittle material should be added to the jar to serve as a chopper and prevent from cold-welding of the ductile materials. Using this method, one can obtain nanoparticles of ductile materials by ball milling [1–5]. The brittle choppers also undergo size reduction down to nano size during the ball milling. Thus, they are referred to as nanochoppers in this chapter.

Along with their brittle nature, the nanochoppers should also meet some other requirements. They, for example, must not react with the starting materials. They should be harder than the starting materials, nontoxic, abundant, and economic. However, nanochoppers must have another characteristic which is of great importance: they must be easy to remove from the product, leaving no vestige.

Consequently, the overall process of obtaining nano-sized powders of ductile materials consists of two steps. The first step is ball milling of the starting materials together with a brittle material, and the second step is removal of the brittle material from the product. The latter step, however, may be accomplished by different techniques depending on the characteristics of the brittle material and ultimate objective of producing the powder. The next three sections of this chapter consider the method according to the final purpose of the ball milling: production of metal nanoparticles, production of hydrogen by means of metal nanoparticles, and production of metal oxide nanoparticles.

2. Mass production of nanoparticles of ductile materials

When one's final objective is to produce nanoparticles of a ductile metal, conventional ball-milling procedure may not come in handy as it fails to downscale the ductile metal particles. At the beginning of ball-milling process, the bulk material is fractured into smaller pieces under the pressure of the balls. However, the rate of size reduction of particles decreases as the time passes and eventually approaches to zero [6]. That is, the further ball milling does not lead to smaller particles because the rate of fracture is very low and is almost equal to the rate of cold-welding. There are several reasons for low rate of size reduction after long time. Firstly, fine particles are very unlikely to be entrapped between two balls, and if they are, the stresses exerted from the balls do not break them into pieces. Instead, the ductile particles are

only kneaded and deformed or are thrust into each other to make a larger particle. Also, the intersection of the balls is too large (compared to the size of the particles) to rip the particles apart. When the balls are rolling against each other, they buffet the particles about, making them more susceptible to agglomerate. Under such circumstances, one should add balls with radii comparable to the size of the particles. In practice, particles of a harder, brittle material can play the role of the tiny balls. If a brittle material is added to the jar at the beginning of the ball-milling process, then it is also ground into smaller pieces, and after adequately long time, the brittle particles are nano-sized and act as nanochoppers. These nanochoppers cut the ductile particles into pieces and reduce their sizes.

Some practical instances of application of this method are introduced here. First, we show how to prepare graphene nanoflakes, and then we report the experiment conducted to extend the methodology to mass production of aluminum nanoparticles.

2.1. Preparing graphene nanoflakes

Graphene has a two-dimensional, hexagonal lattice that is composed of sp²-bonded carbon atoms [1, 7, 8]. It was first invented through micromechanical cleavage of graphite in 2004 [9], and its extraordinary characteristics [10, 11] have drawn the scientists' and engineers' attentions toward its promising applications in different fields such as composite materials, transparent conductive films, ultrasensitive gas sensors, and solar cells [12–14]. Various methods for producing graphene flakes have so far been invented which are commonly categorized into two groups: bottom-up and top-down methods. In bottom-up methods, the hexagonal carbon structure is formed from molecular precursors (e.g., epitaxial growth of graphene on substrates) [15, 16] and thermal decomposition of SiC [17]. These production processes, however, are very energy-consuming, and their yield is low. They also need expensive equipment. In the methods classified as top-down group, on the other hand, graphene layers are peeled out or extracted off the graphitic microstructures such as carbon nanotubes, carbon fibers, and graphite (or graphite oxide) by chemical, electrochemical, or physical techniques [18–20]. These techniques typically include complicated syntheses, harsh oxidizers [21], or immoderate utilization of organic solvents for exfoliation [22–24]. To produce graphene flakes in larger quantities, one may also choose mechanical milling method because it is relatively convenient and economic. However, if graphite powder is solely ground in a planetary ball mill, then the milling process augments the stress in the graphite structure [25–27]. Wet environments, on the other hand, degrade the quality of the product because liquid solution in the jar may react with the balls and the jar leaves some impurities in the product [28]. Nevertheless, as explained above, there is a convenient method for reducing the size of graphite particles incessantly by addition of a brittle material to the planetary ball mill. Owing to its convenience and low cost of involved materials, this approach can be easily scaled up.

Sodium chloride (NaCl) is used as the brittle material for ball milling of natural graphite powder. NaCl is added directly to the jar with graphite and ball milled for 2–5 h. The ball-milling process specifications are listed in **Table 1**. The resultant powder is then leached with copious amount of water in ultrasonic bath and then dried at 80°C under vacuum.

NaCl to graphite molar ratio	3
Ball-to-powder weight ratio	20
Rotational speed of the planetary ball mill	350 rpm
Atmosphere	Argon
Atmosphere pressure	0.4 MPa
Ball-milling duration	2–5 h

Table 1. Ball-milling specification for preparing graphene nanoflakes.

The structural and morphological characteristics of a powder milled under abovementioned condition are reported to be as follow:

Figure 1 demonstrates the XRD pattern of the graphite powder milled together with NaCl (the salt is removed by water). The diffraction peak (002) at $2\theta = 26^\circ$ corresponds to a d-spacing of 0.34 nm that approximately matches the graphite (JCPDS No. 75–1621). The width broadening of the peak may be attributed to the lattice strain and size reduction of the particles.

TEM image of the produced graphene is shown in **Figure 2**. One may easily recognize the distinct layers of graphene (with approximate size of $200 \times 50 \text{ nm}^2$). As seen in the figure, the graphene flakes have ragged edges which are cut off by brittle salt particles.

Figure 3 shows the topology of the graphene powder obtained by AFM that, consistent with TEM image, confirms the ragged edges of the graphene layers.

Specific surface area of the graphene flakes produced by brittle-ductile milling technique is reported to be $524.4 \text{ m}^2/\text{g}$. This value is close to that of the graphene nanoflakes obtained using chemicals and microwave radiation, as reported by Sridhar et al. [29].

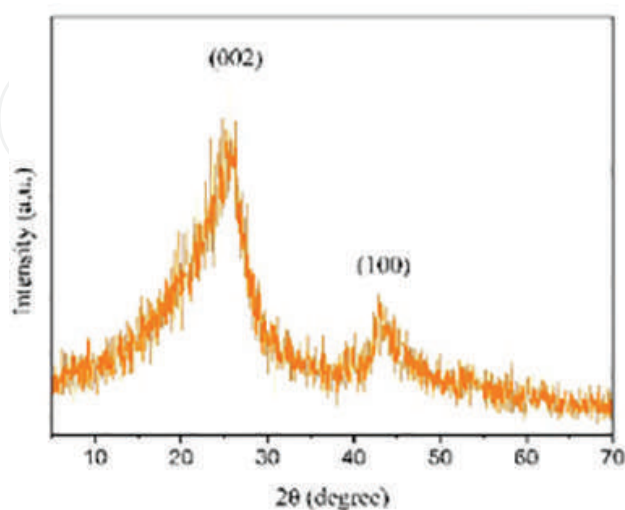


Figure 1. XRD pattern of graphite powder that is milled together with salt (salt is then washed away by water). Source: Ref. [1], Copyright © 2017 Word Scientific.

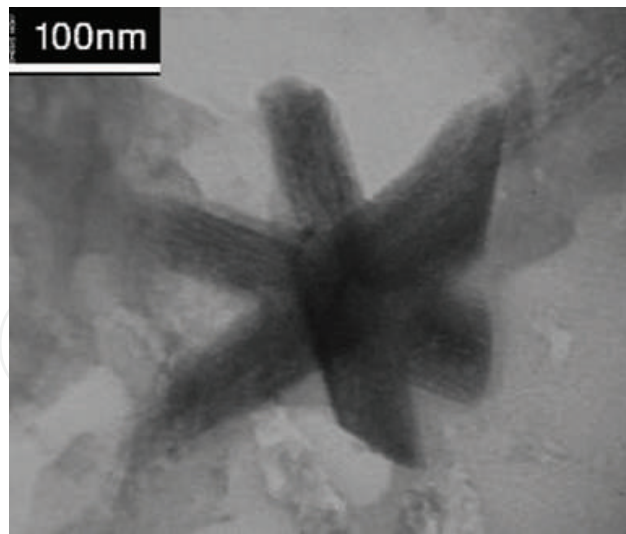


Figure 2. TEM image of graphene powder after 2 hours of milling with NaCl (salt is removed by water). Source: Ref. [1], Copyright @ 2017 Word Scientific.

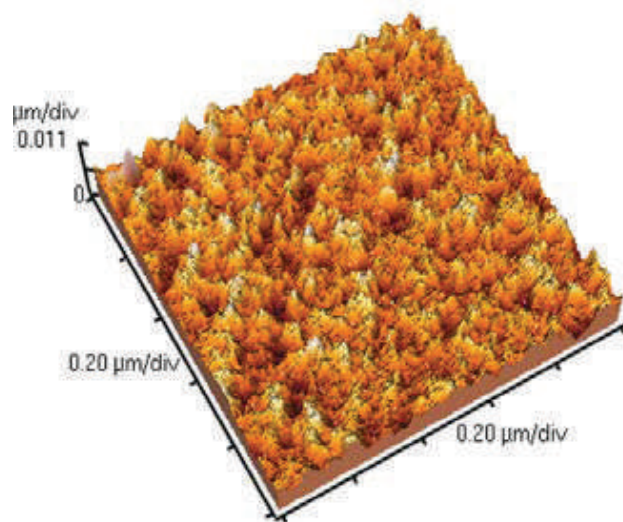


Figure 3. AFM image of the graphene flake. Source: Ref. [1], Copyright @ 2017 Word Scientific.

The average size of the particles reduces from 200 to 400 nm to about 50–150 nm as the ball-milling duration increases from 2 to 5 h. Size of salt particles also decreases during the ball milling [2] as shown in **Figure 4**. Average size of salt particles is reported to be about 150 nm after 5 h of ball milling. Owing to their brittle nature, salt particles fracture and take sharp edges by which they can cut graphite particles into smaller pieces. High salt-to-graphite molar ratio (3,1), on the other hand, retards the agglomeration of graphene flakes.

Moreover, graphene layers are exfoliated due to the shear stress caused by random multiaxial collision of the balls which is also assisted by salt particles. Because of the random nature of the collisions and the random shape and position of the salt particles, they may exert either compressive forces that chop the graphene particles into smaller pieces or shear forces that exfoliate the layers (**Figure 5**).

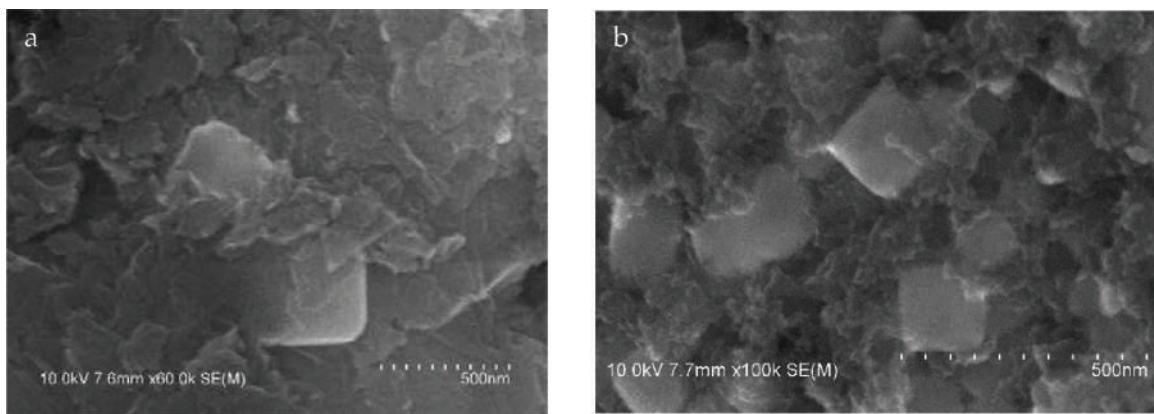


Figure 4. SEM images of graphite powder that is milled together with salt for (a) 2 h and (b) 5 h [1]. Source: Ref. [1], Copyright @ 2017 Word Scientific.

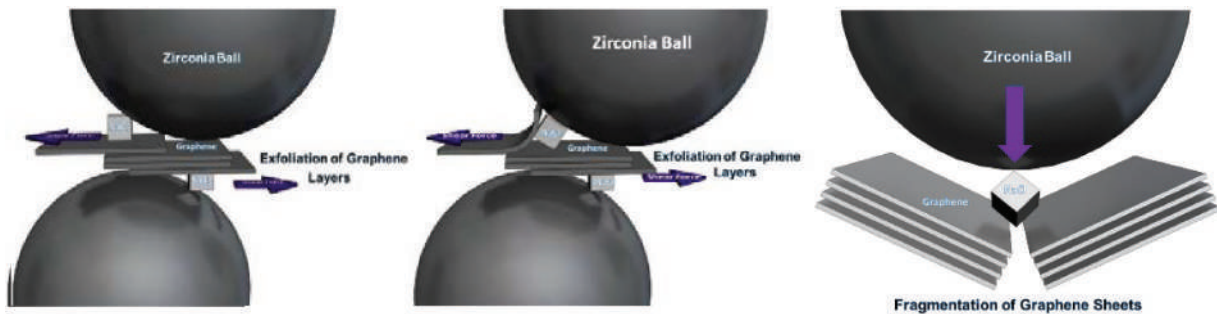


Figure 5. Exfoliation and fragmentation of graphene. Source: Ref. [1], Copyright @ 2017 Word Scientific.

As a nanochopper, salt meets almost all the requirements: it is not expensive, nor toxic; it is abundant and can be easily recycled; and, above all, it conveniently leaches out to water. Hence, this method can be employed for mass production of graphene nanoflakes because it is simple, eco-friendly, and economic.

2.2. Preparing nanoparticles of aluminum

The popularity and importance of aluminum nanoparticle are well understood by knowing its wide application in propellants and pyrotechnics. The methods of manufacturing aluminum nanoparticle are generally classified into two categories: methods involving vapor phase condensation and liquid phase chemistry. One of the vapor phase condensation methods is exploding electronically heated wires [30]. Aluminum nanoparticles, for example, are produced by condensing aluminum vapor generated by passing a strong electrical current through a thin aluminum wire. Some other techniques are occasionally used to prepare metal vapor, namely, radiative heaters, induction heaters or plasma, lasers, and electric arcs. All these techniques require a neutralized gaseous environment whose pressure strongly affects size distribution of resultant nanoparticles. At low pressures, condensation leads to formation of nano-scaled particles. The higher the pressure, the larger the particles. On the other hand, increasing the pressure increases the yield [31]. The effects of other experimental parameters, such as gaseous environment and electric pulse characteristics, are elaborately reported in [31].

All abovementioned techniques suffer from some disadvantages. Production rate is generally low in all of them. Moreover, distribution of particles size extends over a broad range from 10 nm to microns depending on the energy given to the metal. The higher the energy, the wider the distribution. On the other hand, higher energy is required for increasing the yield. This implies that there is a trade-off between the yield and size uniformity. Of course, a narrower range (i.e., uniform distribution of the particle sizes) is generally preferred.

Variations of the bulk aluminum heating technique are reported in [32] in which aluminum is ablated by an Nd-YAG laser.

The other methods of metal nanoparticle production (commonly referred to as liquid phase chemistry) are more chemical. Like all other liquid phase chemistry techniques, measured amount of starting solutions are mixed and stirred slowly, and then the product is dried. As the process is time-consuming, the methods are not appropriate for mass production. In practice, the methods require essential modifications to be qualified enough for producing nanoparticles in large quantities.

Inspired from the method introduced above for preparing graphene nanoflakes, we conducted series of experiments for preparing aluminum nanoparticles. Again, salt was used as the brittle material to serve as nanochopper. Following is the report of the experiments:

Elemental Al powder (99% purity, particle size <100 μm , Fluka) and NaCl (100–200 μm) were ground in a planetary ball mill. The jar of the ball mill was a 125 mL stainless-steel jar with radius of 15 cm. **Table 2** summarizes the specifications of the ball-milling process. The salt-to-aluminum molar ratio (hereafter denoted by η) was 2. To compare the effect of salt particles on size reduction of aluminum particles, the experiment was repeated without salt ($\eta = 0$).

After the milling process accomplished, the salt particles were washed away by immersing the powders in pure water. To prevent aluminum from reacting with water, the process of salt removal was performed using cold water at 1°C and as fast as possible. Resultant aluminum powders were characterized by scanning electron microscopy (SEM, Cambridge S 360) and X-ray diffraction (XRD, Philips 3710 W X-ray diffractometer with CuK α , $\lambda = 1.54184 \text{ \AA}$). The specific surface area of the powders was determined by means of nitrogen adsorption using Brunauer-Emmett-Teller method (BET-N₂, Micrometrics Gemini 2375).

As demonstrated in **Figure 6a**, ball-milling aluminum without salt ($\eta = 0$) has eventually reduced the size of particles to 10 μm . However, the morphology of particles is laminar and

NaCl to aluminum molar ratio (η)	0 and 2
Ball-to-powder-weight ratio	10
Rotational speed of the planetary ball mill	270 rpm
Atmosphere	Argon
Atmosphere pressure	0.4 MPa
Ball-milling duration	20 h

Table 2. Ball-milling specification for preparing aluminum nanoparticles.

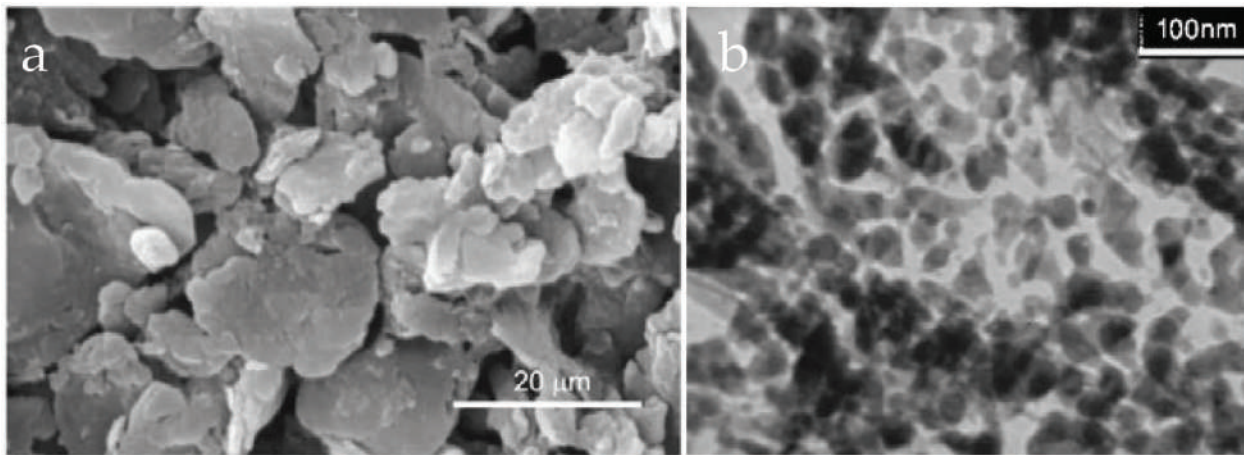


Figure 6. TEM image of ball-milled aluminum particles without (a) and with (b) salt, after removing the salt particles by cold water. Source: Reprinted from Ref. [5], Copyright 2009, with permission from Elsevier.

wrinkled. To reduce the size of the particles, aluminum was milled with high molar ratio of salt ($\eta = 2$). This helps aluminum particles to reach smaller sizes. Salt particles have sharp edges and are hard enough to chop aluminum particles. Due to their brittle nature, they fracture and break into smaller particles during the milling process and cut aluminum particles. Meantime, because of high η , there is a little chance for aluminum particles to meet and cold-weld. **Figure 6b** shows the micrograph of aluminum powder milled together with salt. The size of aluminum particles is decreased to less than 50 nm. Specific surface area of the powder is about 40.9 m²/g.

Aluminum particles prepared by other methods have a hard aluminum oxide crust, while this method leads to nanoparticles with a soft aluminum hydroxide crust which is expected to show better mechanical, consolidation, and sintering behavior. Furthermore, nanoparticles produced by this method have higher lattice residual strain (cf. Section 3 of this chapter). Consequently, the aluminum nanoparticles are more active because mechanical milling causes various defects (dislocations, vacancies, grain boundaries, etc.) in them.

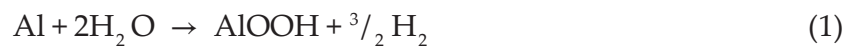
3. Production of hydrogen using metal nanoparticles

Environmental pollutions are one of the most serious challenges during the recent decades, and fossil fuels have the most contribution in the crisis [2]. On the other hand, fossil fuels are not renewable and will run out sooner or later. Consequently, the energy crisis has drawn scientists' attention to eco-friendly and recyclable fuels. One of the best candidates is hydrogen which is currently produced through various methods such as biological [33], water electrolysis [34], and chemical methods [35]. These methods suffer from some disadvantages: they are costly, they have typically low efficiency, and they consume fossil fuels which are neither clean nor recyclable [36, 37].

Another challenge with hydrogen as a fuel is its storage. Since the volumetric density of hydrogen is low, it needs very large storages (at 700 bars, volume of storage required for hydrogen is

about six times that for gasoline with the same energy content). The ignition energy of hydrogen, on the other hand, is 0.03 mJ, implying that it is extremely flammable [38], a fact that must be considered in designing hydrogen storage. Thus, it sounds quite reasonable idea to eliminate the need for the storage by producing hydrogen on demand. There are some hydrogen resources in the nature from which hydrogen may be extracted through a chemical process. Among all, water is the best candidate because its hydrogen content is relatively high (111 kg/m³), it is abundant in nature, it is not costly, and it can be recycled by hydrogen combustion.

The chemical reaction through which hydrogen is obtained from water is simple: oxidation of the active metals. The only challenge is to find proper metal. According to Kravchenko et al., aluminum is the most eligible metal [39], because it is recyclable, it is the most abundant metal in the earth's crust, and its density is very low compared to other metals. The chemical reaction between aluminum and water is as follows:



As seen, the byproduct of the reaction is aluminum oxide hydroxide which is eco-friendly and has many applications (e.g., water conditioning, papermaking, alumina production, fire prevention, and so on).

In normal condition, however, reaction (1) cannot proceed because there is a passive layer of aluminum oxide over the aluminum particles, preventing the inner aluminum atoms from reaction with water. Some solutions to the problem has been so far proposed, each of which having its own disadvantages. Immersing the aluminum in NaOH, for instance, removes the aluminum oxide layer; but it is intensely corrosive and may corrode the instruments [40–42]. Amalgamation of aluminum is another suggestion, but it involves dampening of aluminum surface with eutectic gallium-indium or mercury which are toxic and/or costly [43].

Another method for continuous hydrogen generation from aluminum is using aluminum powder with adequately small particles. This implies higher specific surface area of the powder and, consequently, more activity of the aluminum powder [44, 45]. As explained in the previous section, ordinary ball milling is unable to reduce the size of aluminum particles down to nano size because aluminum is a ductile metal. Even milling the aluminum particles together with brittle hydrides and salts (e.g., MgCl₂, KCl, NaCl, CaH₂, and MgH₂) with brittle-to-ductile molar ratios less than 0.1 has reportedly failed to decrease the size of the aluminum particles [46]. Also, grinding aluminum metallic composites (e.g., aluminum-bismuth) together with inorganic salts only leads to galvanic corrosion and ionic conductivity. This method provides the energy required for the reaction by the heat emerged from exothermic solution of salt. In spite the fact that the method is efficient in energy consumption, it is still ineffective in particle size reduction [46, 47], and moreover, the involved materials are costly, corrosive, and toxic.

As described in the previous section for preparing the aluminum nanoparticles, NaCl is added to the ball mill to serve as nanochopper because it is accessible, economic, easily soluble in water, nontoxic, and eco-friendly. However, η should be much higher than the reported values. Higher η (up to 15 times those reported in [46]) not only reduced the size of the aluminum particles but also increases defects in aluminum crystal by embedding salt gates [2].

As a result, specific surface area of the powder increases drastically, and reaction (1) can proceed until all aluminum content is consumed.

Since the method is simple and involves accessible materials (aluminum, salt, and water), it may be conveniently used for on-demand hydrogen generation:

For generating hydrogen from aluminum nanoparticles, one may start from elemental Al powder and ordinary salt, NaCl (100–200 μm). The mixture of aluminum and salt should be ball milled for 20 h. Ball-milling specifications are summarized in **Table 3**. The η may be selected to be as low as 0.2, but higher η leads to better result. After the milling process, about 150 mL water at a temperature of 70°C is added to the jar. Hydrogen is then released that should be condensed and dried for designated usage.

Figure 7 shows the yield of the reaction (1) as a function of time elapsed after adding water to the jar for different η 's. As one may see in the figure, the efficiency of the samples with more

NaCl to aluminum molar ratio (η)	0.1, 0.2, 0.5, 1.0, and 1.5
Ball-to-powder weight ratio	20
Rotational speed of the planetary ball mill	270 rpm
Atmosphere	Argon
Atmosphere pressure	0.4 MPa

Table 3. Ball-milling specification for preparing aluminum nanoparticles for hydrogen generation.

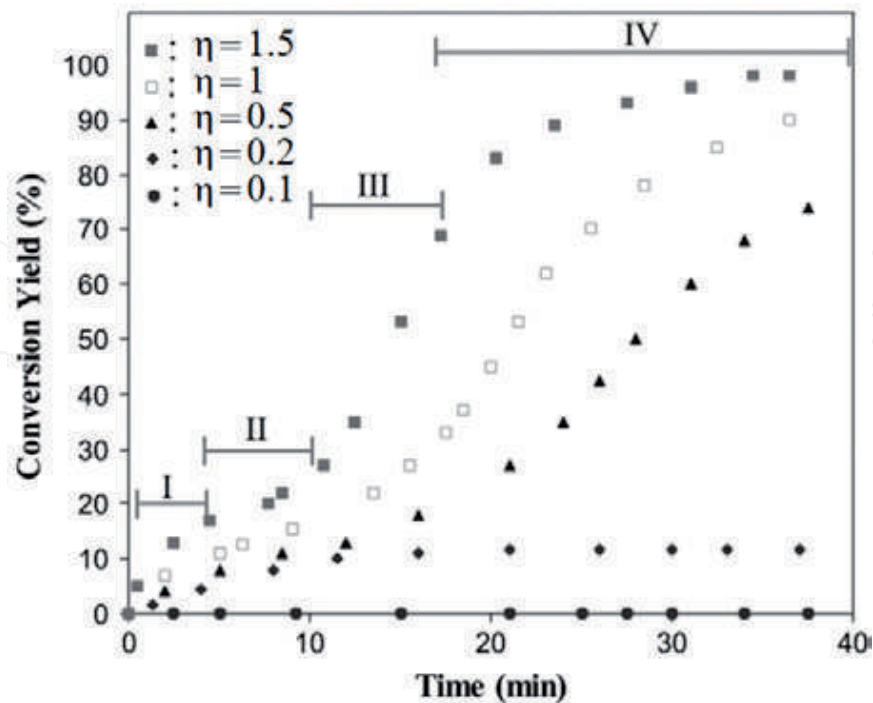


Figure 7. Conversion yield as a function of reaction time for samples with different η . Source: Reprinted from Ref. [2], Copyright 2009, with permission from Elsevier.

salt content is higher. The reaction time may be divided into four regions: In the first region, about the first 5 minutes of milling, hydrogen is mainly generated from the hydration of fresh surfaces. The higher the η in this region, the faster the reaction. This is mainly because smaller particles imply higher specific surface area. The reaction slows down as the passive AlOOH layer is formed over the surface of the particles (region II). The reaction accelerates again in region III when the salt gates dissolve, exposing fresh aluminum to water and letting water to penetrate to the core of the particles. The higher the η , the more surface of fresh aluminum and, hence, the more hydrogen generation. When all the fresh surfaces undergo the reaction, the passive AlOOH layer will eventually hinder the reaction (region IV). Almost all the aluminum atoms in the sample ball milled with $\eta = 1.5$ have undergone the reaction, while ball milling with $\eta = 0.1$ has no considerable effect on the yield. The highest rate of hydrogen generation happens in region III of the sample with $\eta = 1.5$ (75 mL/min per 1 gr of Al).

Unlike other methods (based on hydrogen generation using aluminum in which hydrogen generation is stopped when aluminum particles are covered by a layer of aluminum oxide), all the aluminum contents react with water when the particles are adequately small.

Continuous hydrogen generation may be explained as follows: Salt particles cut the aluminum particles and form local gates on the newly exposed surfaces. They also fracture into smaller particles during the ball milling due to their brittle nature. Salt particles have sharp edges and are harder than aluminum particles. During the ball milling, they rip through aluminum particles making local gates in them. When the salt particles are washed away, fresh surfaces are exposed to water.

Figure 8 is a SEM image of a salt particle among the aluminum particles for a sample with $\eta = 0.5$. Adding more salt to the jar in ball milling (i.e., higher η), of course, leads to development of more salt gates. Thus, higher η rises the kinetics of hydrolysis reaction by increasing the specific surface area of the aluminum particles in two ways: reducing the size of aluminum particles and developing salt gates in them.

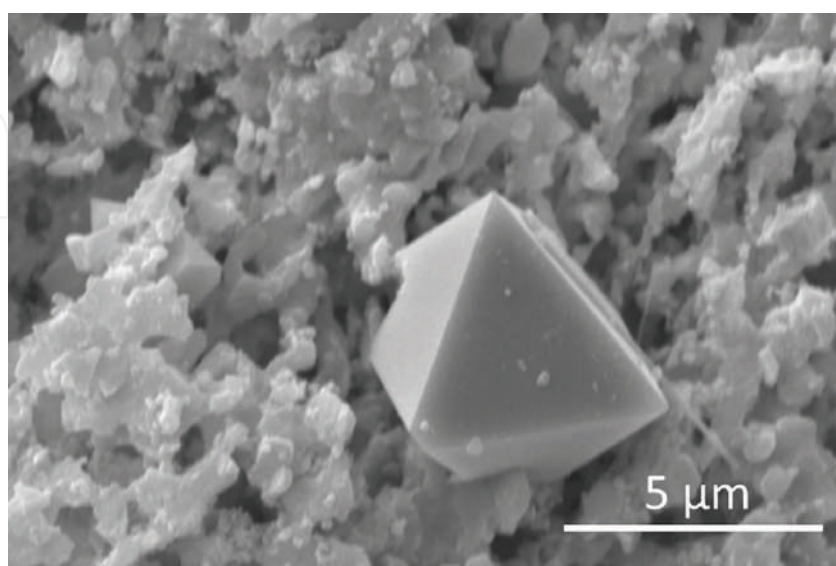


Figure 8. Salt nanochoppers in the context of aluminum nanoparticles. Source: Reprinted from Ref. [2], Copyright 2009, with permission from Elsevier.

It is worth mentioning that there are, of course, some inhibitors (e.g., stearic acid) that are assumed to prevent cold-wedding. However, they evaporate during the ball-milling process which relatively takes a long time. Therefore, they do not practically avoid the cold-welding in long-time ball milling. Furthermore, since the inhibitors are greasy, they prevent aluminum particle from reacting with water. Using salt brittle particles (with $\eta > 1.5$), one can obtain aluminum powder with particle size of about 50 nm and specific surface area of 40.9 m²/g. This means that water can reach to the core of the particles and the reaction can proceed to release their innermost hydrogen contents. Moreover, mechanical milling gives rise to various defects in aluminum particles such as vacancies, dislocations, grain boundaries, etc.

Table 4 summarizes the lattice strain and crystallite size of the powders. The values are calculated by line broadening of XRD peaks and Williamson-Hall technique. This table suggests that adding salt to the ball mill increases the lattice strain, the fact that is also supported by XRD patterns of the samples milled with and without salt. **Figure 9** shows the XRD pattern of the samples ball milled with $\eta = 0$ (no salt) and $\eta = 1.5$. The inset in this figure magnifies the

η	Crystal structure (Å)	Crystalline size (nm)	Lattice strain (%)
0.0 (no salt)	Cubic (a = 4.046(2))	42.22(1)	0.61(4)
1.5	Cubic (a = 4.44(3))	43.13(3)	0.50(1)

Source: Reprinted from Ref. [2], Copyright 2009, with permission from Elsevier.

Table 4. Crystalline characteristics of aluminum powders milled with $\eta = 0$ (no salt) and $\eta = 1.5$.

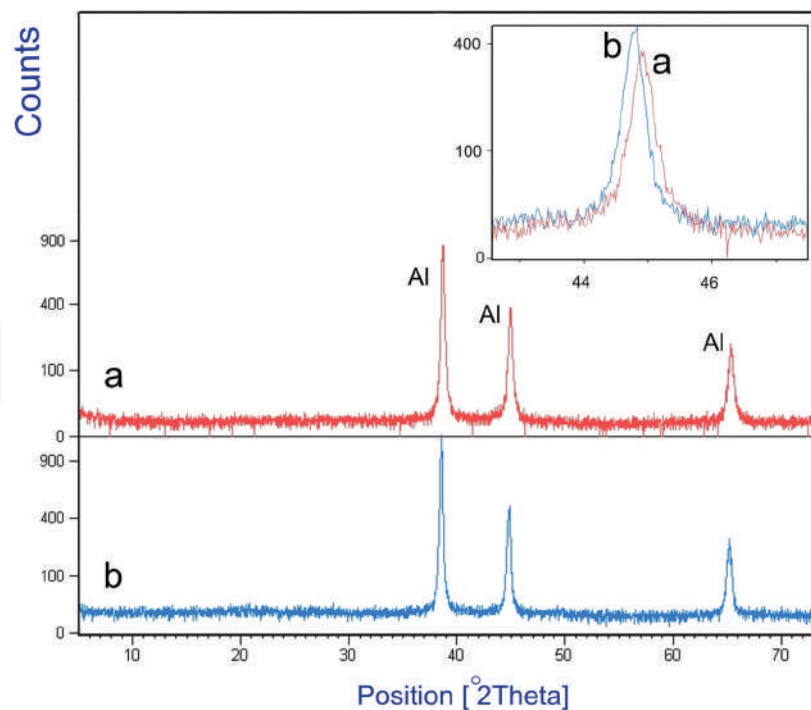


Figure 9. XRD pattern of the samples ball milled with $\eta = 1.5$ (a) and $\eta = 0$ (no salt) (b). The inset magnifies the shift of (200) peaks in the samples. Source: Reprinted from Ref. [2], Copyright 2009, with permission from Elsevier.

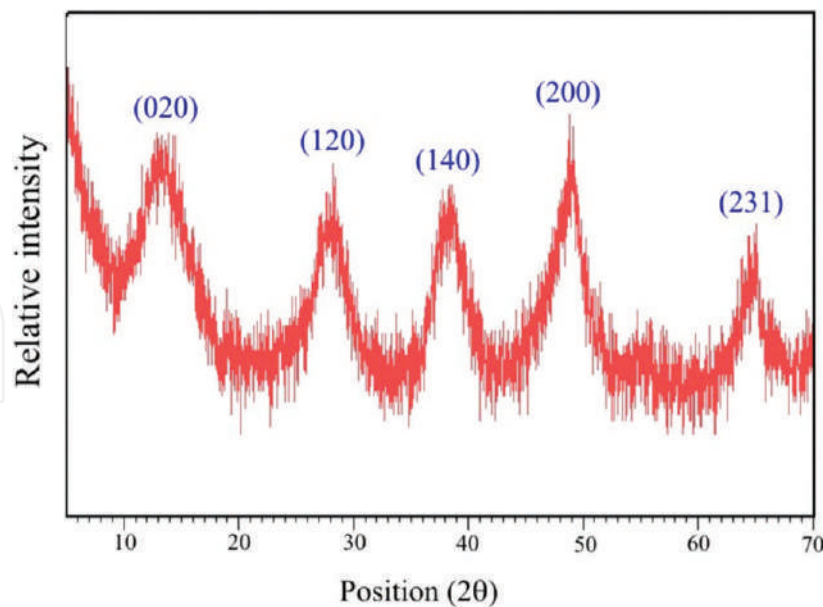


Figure 10. XRD pattern of the sample ball milled with $\eta = 1.5$ after reacting with hot water. The peaks correspond to AlOOH , and there is no evidence of aluminum. Source: Reprinted from Ref. [2], Copyright 2009, with permission from Elsevier.

XRD differences of the two samples. The lattice strain developed by ball milling provides a driving force that results in more corrosion or oxidation [14].

On the other hand, aluminum-water reaction is exothermic which helps the reaction proceed spontaneously. During hydrolysis, water temperature increases from 70°C to maximum of 74°C . Release of hydrogen in the interface of aluminum and aluminum hydroxide gel increases the porosity, letting water penetrate deep inside the aluminum particle and react with innermost atoms. X-ray diffraction pattern of the powder milled with $\eta = 1.5$ after reacting with hot water is shown in **Figure 10**, which is in good agreement with the characteristic spectrum of AlOOH crystal in the JCPDS database, except for the broader peaks due to a lower crystallinity. Aluminum is absent in the diffraction pattern, implying that reaction has reached the core of aluminum particles and entire aluminum powder has turned into AlOOH .

4. Production of metal oxide nanoparticles

The same method as explained above may be employed to prepare nanoparticles of ductile metal oxides. To examine the method for a different ductile metal, we selected a metal that its oxide is of great importance and has many applications: zinc oxide.

Even in its bulk state, zinc oxide has interesting properties: it is electrically stable with a direct band gap of 3.37 eV ; it is transparent for visible light; it is abundant and nontoxic. Owing to its fabulous properties, it is widely used in various field of industry such as sensors, optoelectronic devices, solar cells, catalysts, field emission, data storage, etc. [48, 49]. On the other hand, due to its hexagonal Wurtzite structure and polar crystal surfaces, zinc oxide can take

on different nanostructures (e.g., nanorods, nanotubes, nanobelts, and nanosheets) only by restraining certain direction(s) from growing [50, 51]. The methods by which one can produce the different nanostructures are generally categorized into two groups: vapor phase process and solution phase route. The first group consists of physical vapor of the deposition, vapor phase transport and some other methods [52]. All these methods, however, have some disadvantages in common. They, for instance, require high temperatures to accomplish. Also, they need costly equipment and accomplish only when some strict conditions are all met. They sometimes employ metal catalysts (e.g., gold) to control the growth process [53]. Solution phase route group (including sol-gel and hydrothermal methods [54]) suffer from some disadvantages too: they are time-consuming and require costly chemicals. They also employ some toxic, dangerous and expensive organic solvents amine in solvothermal process.

The simplest method for producing zinc oxide is the direct reaction between zinc and water. However, as with aluminum, a thin layer of zinc oxide is formed all over the zinc particle, preventing from the reaction. Although some techniques have been proposed so far, none can synthesize zinc oxide incessantly. Using zinc foil as a substrate for growing zinc oxide, for instance, leads to formation of a thin layer of zinc oxide [55]. Another suggested method is oxidation of zinc nanoparticles. If average radius of particles is smaller than thickness of the zinc oxide layer (about 10 nm), then this method works; otherwise, the particle is coated with a zinc oxide layer hindering the core of particle from oxidation [56].

In our experiment, we tried to reduce the size of the particles (or, in other words, activate them). The activation may be performed by milling zinc powder with high molar fraction of salt (as described in previous sections). This not only reduces the size of zinc particles but also covers newly produced surfaces with salt particles that otherwise would be covered by zinc oxide layer. So, the product can be stored in the air needing no neutral gas. When the salt is leached, fresh surfaces of zinc are exposed to water. Then, all nanoparticles react with water, entirely. Instead of using zinc salts (e.g., $\text{Zn}(\text{CH}_3\text{COO})_2 \cdot 2\text{H}_2\text{O}$) and other chemicals (e.g., NaOH, KOH, etc.) or alcohol solutions (that are employed in preparing some metal oxides), only zinc, salt and water are utilized in this method. This method is highly efficient and eco-friendly and does not need costly, complex equipment. It can be employed to manufacture other metal oxide systems [5] and scaled up for mass production.

Following is the report of experiment:

Zn powder (99% purity, Mesh-325, Merck Art.No. 1.08789) and salt (100-200 μm) were ground in a planetary ball mill with the specification tabulated in **Table 5**. The ground powder was poured in 250 mL of water at 75°C and was stirred by a magnetic stirring machine at constant temperature for 5 h. The powder was then washed before being dried in an oven at 80°C and before being characterized by X-Ray Diffraction (XRD, using Philips 3710W X-Ray diffractometer with $\text{CuK}\alpha$ ($\lambda = 1.54184 \text{ \AA}$) radiation), Scanning Electron Microscopy (SEM, using Cambridge S 360) and Transmission Electron Microscopy (TEM, using Philips EM 208S). Specific surface area of the powder was determined through nitrogen adsorption by Brunauer-Emmett-Teller method (BET- N_2 adsorption, Micromeritics Gemini 2375).

Figure 11 shows X-ray diffraction profile of resultant zinc oxide powder. The peaks corresponding to hexagonal phase of ZnO (JCPDS 36-1451) are illustrated. Sharp peaks signify good crystallinity of zinc oxide powder. Lattice constants ($a = 3.2543(1) \text{ \AA}$ and $c = 5.2134(2) \text{ \AA}$)

NaCl to zinc molar ratio	5
Ball-to-powder weight ratio	30
Rotational speed of the planetary ball mill	300 rpm
Atmosphere	Argon
Atmosphere pressure	0.4 MPa

Table 5. Ball-milling specification for preparing ZnO nanoparticles.

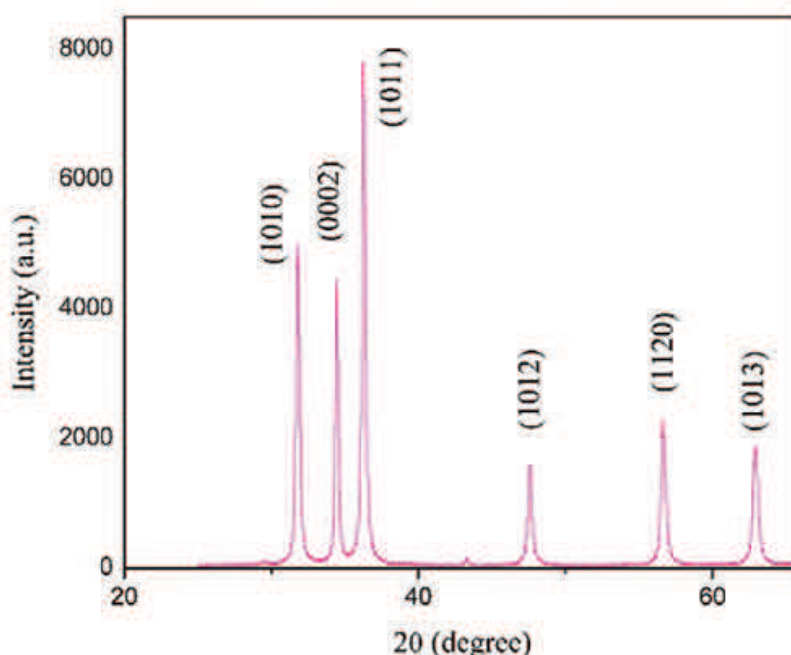


Figure 11. XRD pattern of zinc oxide powder obtained by reaction with water.

were slightly larger than those reported in corresponding JSPDS card number for bulk ZnO ($a = 3.2498 \text{ \AA}$ and $c = 5.2066 \text{ \AA}$).

Zinc oxide particles obtained by this method are of two different morphologies: hexagonal flakes and rod structure. Depicted in **Figure 12a** is SEM of densely stacked hexagonal flakes. The average size of flakes is 200 nm. **Figure 12b** shows the TEM image of the second morphology (rod structure) with average length and diameter of 100 and 20 nm, respectively. Selected-Area Electron Diffraction (SAED) pattern of the powder is depicted just below **Figure 12b**. It can be indexed as hexagonal Wurtzite-structural ZnO, which is consistent with the analysis of XRD. The specific surface area of the powder obtained in our experiment was $18.25 \text{ m}^2/\text{g}$. It is, of course, a function of ball-milling specifications.

Theoretical explanation of the mechanism of synthesizing zinc oxide by abovementioned method may be represented as following: zinc atoms react with water to give zinc oxide. However, this happens only for the outermost atoms of a zinc particle because the zinc oxide (or zinc hydroxide) crust prevents water from diffusing into the particle, and consequently, inner atoms do not react with water. If the powder is milled together with brittle particles

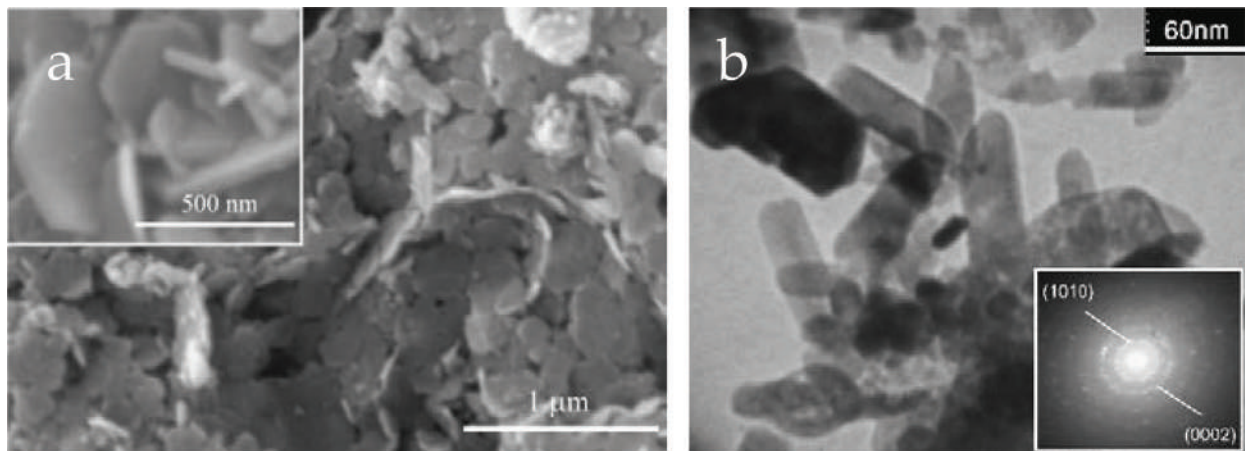


Figure 12. (a) SEM image of ZnO powder and (b) TEM image of ZnO powder and its corresponding SAED pattern (inset).

of salt, the oxide layer initially formed on the Zn particles is destroyed and newly produced surfaces are immediately covered by salt particles. Therefore, the activity of powder does not decrease after long-term storage in the air. When the powder is submerged by water, the salt is washed away, and zinc atoms are exposed to water and react with it:



Due to direct contact of zinc atoms with warm water, kinetics of reaction is rapid. Thus, a considerable amount of hydrogen is generated in each particle and in its way out, it burst open the zinc oxide or zinc hydroxide crust, exposing more fresh zinc to water. Hence, provided that zinc particles are small enough, all the contents of zinc is converted to zinc oxide. Zinc hydroxide contents are also hydrated to give zinc oxide as indicated by following reaction:



Unlike reaction (2) that is exothermic, reaction (3) is endothermic [57]. Warm water provides required energy for the reaction. The zinc oxide particles obtained from reaction (3) serve as seeds for agglomeration leading to a planar hexagonal nuclei. Zinc oxide lattice (as suggested by crystal habit of wurtzite ZnO) is composed of tetrahedrons with a zinc atom at the center and four oxygen atoms at the vertices. Hence, the (0001) planes in the hexagonal sheet is zinc-rich while the opposite plane (i.e., $(000\bar{1})(000\bar{1})$) is oxygen-rich. Li et al. put a rule forward according which the fastest growth rate of zinc oxide happens along $[000\bar{1}]$ direction and the rate of growth along other directions obey the following relation [58]:

$$V[0001] > V[01\bar{1}\bar{1}] > V[01\bar{1}0] > V[01\bar{1}1] > V[000\bar{1}] \quad (4)$$

Based on their rule, $\langle 0001 \rangle$ direction is the most preferable direction for zinc oxide nanoparticles to grow or aggregate. Two-dimensional hexagonal structures imply that the growth is hindered in this direction and the crystals grow along $\langle 10\bar{1}010\bar{1}0 \rangle$ direction. This may be due to

resident Cl^- ions. Cl^- ions are adsorbed preferentially on the positive polar face of the (0001) surface, which limits the axis growth along the $\langle 0001 \rangle$ direction and accelerates the radial growth [59]. Thus, the morphology of synthesized particles can be controlled by manipulating the concentration of the ions in the media.

5. Conclusion

A simple method for preparing nanoparticles of ductile metals by means of ball milling was proposed based on the experiments reported by others and experiments conducted by the authors. The essential point of the method is using a brittle material as nanochopper during the ball milling. The method showed to be very useful and leads to good results. In all the cases represented in this chapter, salt was used as the brittle material (the nanochopper). However, other ductile materials may be employed according to the nature of the experiment and ultimate purpose of preparing the nanoparticles.

Author details

Babak Alinejad* and Yazdan Zare

*Address all correspondence to: 16nd114n@vc.ibaraki.ac.jp

Ibaraki University, Hitachi, Japan

References

- [1] Alinejad B, Mahmoodi A. Synthesis of graphene nanoflakes by grinding natural graphite together with NaCl in a planetary ball mill. *Functional Materials Letters*. 2017;**10**(04):1750047. DOI: 10.1142/S1793604717500473
- [2] Alinejad B, Mahmoodi K. A novel method for generating hydrogen by hydrolysis of highly activated aluminum nanoparticles in pure water. *International Journal of Hydrogen Energy*. 2009;**34**(19):7934-7938. DOI: 10.1016/j.ijhydene.2009.07.028
- [3] Mahmoodi K, Alinejad B. Enhancement of hydrogen generation rate in reaction of aluminum with water. *International Journal of Hydrogen Energy*. 2010;**35**(11):5227-5232. DOI: 10.1016/j.ijhydene.2010.03.016
- [4] Mahmoodi K, Alinejad B. Fast and facile synthesis of boehmite nanofibers, powder technology. 2010;**199**(3):289-292. DOI: 10.1016/j.powtec.2010.01.019
- [5] Alinejad B, Mahmoodi K, Ahmadi K. A new route to mass production of metal hydroxide/oxide hydroxide nanoparticles. *Materials Chemistry and Physics*. 2009;**118**(2-3):473-476. DOI: 10.1016/j.matchemphys.2009.08.020

- [6] Suryanarayana C. Mechanical alloying and milling. Marcel Dekker. 2004:87-89. DOI: 10.1080/10426910701416344
- [7] Geim AK, Novoselov KS. The rise of graphene. *Nature Materials*. 2007;6:183. DOI: 10.1038/nmat1849
- [8] Geim AK, MacDonald AH. Graphene: Exploring carbon flatland. *Physics Today*. 2007; 60(8):35. DOI: 10.1063/1.2774096
- [9] Novoselov KS, Geim AK, Morozov SV, Jiang D, Zhang Y, Dubonos SV, Grigorieva IV, Firsov AA. Electric field effect in atomically thin carbon films. *Science*. 2004;306(5696):666-669. DOI: 10.1126/science.1102896
- [10] Wang F, Zhang Y, Tian C, Girit C, Zettl A, Crommie M, Ron Shen Y. Gate-variable optical transitions in graphene. *Science*. 2008;320(5873):206-209. DOI: 10.1126/science.1152793
- [11] Lee C, Wei X, Kysar JW, Hone J. Measurement of the elastic properties and intrinsic strength of monolayer graphene. *Science*. 2008;321(5887):385-388. DOI: 10.1126/science.1157996
- [12] Robinson JT, Keith Perkins F, Snow ES, Wei Z, Sheehan PE. Reduced graphene oxide molecular sensors. *Nano Letters*. 2008;8(10):3137-3140. DOI: 10.1021/nl8013007
- [13] Blake P, Brimicombe PD, Nair RR, Booth TJ, Jiang D, Schedin F, Ponomarenko LA, Morozov SV, Gleeson HF, Hill EW, Geim AK, Novoselov KS. Graphene-based liquid crystal device. *Nano Letters*. 2008;8(6):1704-1708. DOI: 10.1021/nl080649i
- [14] Ji Z, Shen X, Song Y, Zho G. In situ synthesis of graphene/cobalt nanocomposites and their magnetic properties. *Materials Science and Engineering B*. 2011;176(9):711-715. DOI: 10.1016/j.mseb.2011.02.026
- [15] Reina A, Jia X, Ho J, Nezich D, Son H, Bulovic V, Dresselhaus MS, Kong J. Large area, few-layer graphene films on arbitrary substrates by chemical vapor deposition. *Nano Letters*. 2009;9(1):30-35. DOI: 10.1021/nl801827v
- [16] Sutter PW, Flege J, Sutter EA. Epitaxial graphene on ruthenium. *Nature Materials*. 2008;7:406-411. DOI: 10.1038/nmat2166
- [17] Berger C, Song Z, Li T, Li X, Ogbazghi AY, Feng R, Dai Z, Marchenkov AN, Conrad EH, First PN, de Heer WA. Ultrathin epitaxial graphite: 2D electron gas properties and a route toward graphene-based nanoelectronics. *The Journal of Physical Chemistry B*. 2004;108(52):19912-19916. DOI: 10.1021/jp040650f
- [18] Park S, Ruoff RS. Chemical methods for the production of graphenes. *Nature Nanotechnology*. 2009;4:217-224. DOI: 10.1038/nnano.2009.58
- [19] Kotov NA, Dékány I, Fendler JH. Ultrathin graphite oxide-polyelectrolyte composites prepared by self-assembly: Transition between conductive and non-conductive states. *Advanced Materials*. 1996;8:637-641. DOI: 10.1002/adma.19960080806

- [20] Chandra S, Sahu S, Pramanik P. A novel synthesis of graphene by dichromate oxidation. *Materials Science and Engineering B*. 2010;**167**(3):133-136. ISSN:0921-5107. DOI: 10.1016/j.mseb.2010.01.029
- [21] Zhamu A, Zhang B Z. Environmentally benign graphite intercalation compound composition for exfoliated graphite, flexible graphite, and nano-scaled graphene platelets. US patent claim 20090028778; 2009
- [22] Geng Y, Wang SJ, Kim J. Preparation of graphite nanoplatelets and graphene sheets. *Journal of Colloid and Interface Science*. 2009;**336**(2):592-598. ISSN 0021-9797. DOI: 10.1016/j.jcis.2009.04.005
- [23] Arsat R, Breedon M, Shafiei M, Spizziri PG, Gilje S, Kaner RB, Kalantar-zadeh K, Wlodarski W. Graphene-like nano-sheets for surface acoustic wave gas sensor applications. *Chemical Physics Letters*. 2009;**467**(4-6):344-347. ISSN 0009-2614. DOI: 10.1016/j.cplett.2008.11.039
- [24] Drzal LT, Fukushima H. Graphite nanoplatelets as reinforcements for polymers. *Polymer Preprints (American Chemical Society, Division of Polymer Chemistry)*. 2001;**42**(2):42-43
- [25] Welham NJ, Berbenni V, Chapman PG. Effect of extended ball milling on graphite. *Journal of Alloys and Compounds*. 2003;**349**(1-2):255-263. ISSN:0925-8388
- [26] Wakayama H, Mizuno J, Fukushima Y, Nagano K, Fukunaga T, Mizutani U. Structural defects in mechanically ground graphite. *Carbon*. 1999;**37**(6):947-952. ISSN:0008-6223
- [27] Pierard N, Fonseca A, Colomer JF, Bossuot C, Benoit JM, Van Tendeloo G, Pirard JP, Nagy JB. Ball milling effect on the structure of single-wall carbon nanotubes. *Carbon*. 2004;**42**(8-9):1691-1697. ISSN:0008-6223. DOI: 10.1016/j.carbon.2004.02.031
- [28] Knieke C, Berger A, Voigt M, Klupp Taylor RN, Röhl J, Peukert W. Scalable production of graphene sheets by mechanical delamination. *Carbon*. 2010;**48**(11):3196-3204. ISSN:0008-6223. DOI: 10.1016/j.carbon.2010.05.003
- [29] Sridhar V, Jeon J, Oh I. Synthesis of graphene nano-sheets using eco-friendly chemicals and microwave radiation. *Carbon*. 2010;**48**(10):2953-2957. ISSN:0008-6223. DOI: 10.1016/j.carbon.2010.04.034
- [30] Sarathi R, Sindhu TK, Chakravarthy SR. Generation of nano aluminium powder through wire explosion process and its characterization. *Materials Characterization*. 2007; **58**(2):148-155. DOI: 10.1016/j.matchar.2006.04.014
- [31] Meda L, Marra G, Galfetti L, Severini F, De Luca L. Nano-aluminum as energetic material for rocket propellants. *Materials Science and Engineering C*. 2007;**27**:1393-1396. DOI: 10.1016/j.msec.2006.09.030
- [32] El S, Barberoglou M, Fotakis C, Viau G, Garcia C, Shafeev GA. Generation of Al nanoparticles via ablation of bulk Al in liquids with short laser pulses. *Optics Express*. 2009;**17**(15):12650-12659. DOI: 10.1364/OE.17.012650

- [33] Kapdan IK, Kargi F, Oztekin R, Argun H. Bio-hydrogen production from acid hydrolyzed wheat starch by photo-fermentation using different *Rhodobacter* sp. *International Journal of Hydrogen Energy*. 2009;**34**:2201-2207. DOI: 10.1016/j.ijhydene.2009.01.017
- [34] de Souza RF, Padilha JC, Gonçalves RS, de Souza MO, Berthelot JR. Electrochemical hydrogen production from water electrolysis using ionic liquid as electrolytes: Towards the best device. *Journal of Power Sources*. 2007;**164**:792-798. DOI: 10.1016/j.jpowsour.2006.11.049
- [35] Kojima Y, Suzuki K, Fukumoto K, Sasaki M, Yamamoto T, Kawai Y, Hayashi H. Hydrogen generation using sodium borohydride solution and metal catalyst coated on metal oxide. *International Journal of Hydrogen Energy*. 2002;**27**:1029-1034. DOI: 10.1016/S0360-3199(02)00014-9
- [36] Kotay SM, Das D. Biohydrogen as a renewable energy resource—Prospects and potentials. *International Journal of Hydrogen Energy*. 2008;**33**(1):258-263. DOI: 10.1016/j.ijhydene.2007.07.031
- [37] U.S. Department of Energy. Office of fossil energy—Hydrogen Program Plan: Hydrogen from Natural Gas and Coal: the Road to a Sustainable Energy Future. Available from: <https://www.netl.doe.gov/File%20Library/Research/Coal/ccbt/fehydrogenplan2003.pdf> [Accessed March 05, 2018]
- [38] Tzimas E, Filiou C, Peteves SD, Veyret J B. Hydrogen storage: State of the art and future perspective, European Commission, Directorate General Joint Research Centre, Institute for Energy, Petten, the Netherlands. Available from: <https://pdfs.semanticscholar.org/1fc0/398a56d147790df6b8af9aab677e1c04eeb6.pdf> [Accessed: March 05, 2018]
- [39] Kravchenko OV, Semenenko KN, Bulychev BM, Kalmykov KB. Activation of aluminum metal and its reaction with water. *Journal of Alloys and Compounds*. 2005;**397**:58-62. DOI: 10.1016/j.jallcom.2004.11.065
- [40] Hiraki T, Takeuchi M, Hisa M, Akiyama T. Hydrogen production from waste aluminum at different temperatures with LCA. *Materials Transactions*. 2005;**46**(5):1052-1057. DOI: 10.2320/matertrans.46.1052
- [41] Andersen ER, Andersen EJ. Method for producing hydrogen. US Patent 6506360; 2003
- [42] Martínez SS, Sanchez LA, Alvarez Gallegos AA, Sebastian PJ. Coupling a PEM fuel cell and the hydrogen generation from aluminum waste cans. *The International Journal of Hydrogen Energy*. 2007;**32**:3159-3162. DOI: 10.1016/j.ijhydene.2006.03.015
- [43] Parmuzina AV, Kravchenko OV. Activation of aluminum metal to evolve hydrogen from water. *International Journal of Hydrogen Energy*. 2008;**33**:3073-3076
- [44] Ilyin AP, Gromov AA, Reshetov AA, Tihonov DV, Yablunowsky GV. Reactionary ability of aluminum ultrafine powders in various oxidation processes. In: *The 4th Russian-Korean International Symposium on Science Technology KORUS Proceedings*. Vol. 3; 2000. pp. 299-304
- [45] Ivanov VG, Safronov MN, Gavrilyuk OV. Macrokinetics of oxidation of ultradisperse aluminum by water in the liquid phase. *Combustion, Explosion, and Shock Waves*. 2001;**37**(2):173-177

- [46] Fan MQ, Xu F, Sun LX, Zhao JN, Jiang T, Li WX. Hydrolysis of ball milling Al–Bi–hydride and Al–Bi–salt mixture for hydrogen generation. *Journal of Alloys and Compounds*. 2008;**460**:125-129
- [47] Fan MQ, Xu F, Sun LX. Studies on hydrogen generation characteristics of hydrolysis of the ball milling Al-based materials in pure water. *International Journal of Hydrogen Energy*. 2007;**32**:2809-2815
- [48] Liu CH, Zapien JA, Yao Y, Meng XM, Lee CS, Fan SS, Lifshitz Y, Lee ST. High-density, ordered ultraviolet light-emitting ZnO nanowire arrays. *Advanced Materials*. 2003;**15**:838-841. DOI: 10.1002/adma.200304430
- [49] Musić S, Dragčević Đ, Popović S, Ivanda M. Precipitation of ZnO particles and their properties. *Materials Letters*. 2005;**59**:2388-2393. DOI: 10.1016/j.matlet.2005.02.084
- [50] Wang ZL. Nanostructures of zinc oxide. *Materials Today*. 2004;**7**(6):26-33. ISSN:1369-7021. DOI: 10.1016/S1369-7021(04)00286-X
- [51] Kumar S, Kim YJ, Koo BH, Gautam S, Chae KH, Kumar R, Lee CG. Room temperature ferromagnetism in chemically synthesized ZnO rods. *Materials Letters*. 2009;**63**(2):194-196. ISSN:0167-577X. DOI: 10.1016/j.matlet.2008.09.057
- [52] Ouyang W, Zhu J. Catalyst-free synthesis of macro-scale ZnO nanonail arrays on Si substrate by simple physical vapor deposition. *Materials Letters*. 2008;**62**(17-18):2557-2560. ISSN:0167-577X. DOI: 10.1016/j.matlet.2007.12.051
- [53] Nagase M, Suhara M, Miyamoto Y, Furuya K. Peak width analysis of current–voltage characteristics of triple-barrier resonant tunneling diodes. *Japanese Journal of Applied Physics*. 2000;**39**:3314-3318 (Part 1, Number 6A)
- [54] Lepot N, Van Bael MK, Van den Rul H, D'Haen J, Peeters R, Franco D, Mullens J. Synthesis of ZnO nanorods from aqueous solution. *Materials Letters*. 2007;**61**(13):2624-2627. ISSN:0167-577X. DOI: 10.1016/j.matlet.2006.10.025
- [55] Chenglin Y, Dongfeng X. Solution growth of nano- to microscopic ZnO on Zn. *Journal of Crystal Growth*. 2008;**310**(7-8):1836-1840. ISSN:0022-0248. DOI: 10.1016/j.jcrysgro.2007.10.060
- [56] Nakamura R, Lee JG, Tokozakura D, Mori H, Nakajima H. Formation of hollow ZnO through low-temperature oxidation of Zn nanoparticles. *Materials Letters*. 2007;**61**(4-5):1060-1063. DOI: 10.1016/j.matlet.2006.06.039
- [57] Ge J, Tang B, Zhuo L, Shi Z. A rapid hydrothermal route to sisal-like 3D ZnO nanostructures via the assembly of CTA⁺ and Zn(OH)₄²⁻: Growth mechanism and photoluminescence properties. *Nanotechnology*. 2006;**17**(5):1316-1323
- [58] Li W, Shi E, Zhong W, Yin Z. Growth mechanism and growth habit of oxide crystals. *Journal of Crystal Growth*. 1999;**203**(1-2):186-196. DOI: 10.1016/S0022-0248(99)00076-7
- [59] Xu L, Guo Y, Liao Q, Zhang J, Xu JD. Morphological control of ZnO nanostructures by electrodeposition. *Physical Chemistry B*. 2005;**109**:13519-13522. DOI: 10.1021/jp051007b

We are IntechOpen, the world's leading publisher of Open Access books Built by scientists, for scientists

6,300

Open access books available

171,000

International authors and editors

190M

Downloads

Our authors are among the

154

Countries delivered to

TOP 1%

most cited scientists

12.2%

Contributors from top 500 universities



WEB OF SCIENCE™

Selection of our books indexed in the Book Citation Index
in Web of Science™ Core Collection (BKCI)

Interested in publishing with us?
Contact book.department@intechopen.com

Numbers displayed above are based on latest data collected.
For more information visit www.intechopen.com



Abrasive for Chemical Mechanical Polishing

Hong Jin Kim

Additional information is available at the end of the chapter

<http://dx.doi.org/10.5772/intechopen.75408>

Abstract

Chemical mechanical polishing (CMP) is one of the most essential processes in semiconductor manufacturing. Its importance becomes highly underscored at the advanced device toward sub 14 nm scaling. The fundamental mechanism of CMP is to create soften surface layer by chemical reaction and then, mechanical force by abrasive particles remove soften layer. The role of CMP is not only material removal, but also planarization, surface smoothing, uniformity control, defect reduction and more. Moreover, semiconductor yield enhancement is sensitively influenced by CMP processing. Surface scratching, which is generated by CMP in nature, is considered as 'killer defect' in semiconductor manufacturing. Hence, to achieve proper CMP performance without surface scratching, understanding and development of abrasive particles are crucially important. In this chapter, CMP fundamentals, applications and challenges associated with abrasive particle technology including synthesis (up to nanoparticle scale), tribochemical reaction, abrasive surface zeta potential behavior, particle size and its distribution will be discussed.

Keywords: semiconductor manufacturing, chemical mechanical polishing (CMP), slurry, silica abrasive, ceria abrasive, alumina abrasive, advanced abrasive materials

1. Introduction

Chemical mechanical polishing (CMP) has been used for several decades in semiconductor manufacturing since its development at 1980s [1–5]. The original purpose of CMP is to planarize wafer surface both locally and globally, which enable subsequent lithographic patterning with proper depth of focus [1–5]. However, as device shrinkage continues, it has become critical process for device fabrication, and its applications play a pivotal role in semiconductor process since transistor scaling becomes beyond 14 nm [5–9]. The role of CMP and planarized wafer associated with lithography patterning is shown in **Figure 1** schematically [1, 4].

Surface topography hinders conformal deposition of photoresist, leading to distorted patterning. Furthermore, advantages of employment of CMP in semiconductor manufacturing are [4, 5]: (1) elimination of step coverage burden, (2) defect removal from prior process steps, (3) surface smoothing in wafer scale, and (4) enablement of metal gate formation at sub 14 nm device. The fundamental mechanism of CMP process is [1–4]: (1) Material surface becomes soften by chemical reaction with slurry, (2) Mechanical force by abrasive particle in the slurry removes soften layer and step height reduction, (3) Material surface reacts with slurry chemical to make surface soften layer again and repeat (1) – (3). Therefore, chemistry and abrasive particles in the slurry determines CMP performances. This procedure is given in **Figure 2**. With this process, fast material removal across the wafer with planarization can be achieved. From the abrasive perspective, abrasive-wafer contact model on removal rate has been published in many literatures which emphasize abrasive particle size (and size distribution) and shape, and abrasive hardness. Although CMP application had started from planarization of excessed dielectric materials, its utilization have been widely accepted in shallow trench isolation, contact and metal interconnection formation [1–10]. Recently, sub 14 nm semiconductor scaling has developed device integration scheme to 3-dimensional transistor formation such as fin field-effect transistor, therefore device process flow becomes much more complicated than previous device node [6–9, 11, 12]. Hence, application of CMP extends to transistor formation, and importance of CMP process becomes highly underscored.

Figure 3(a) shows polisher equipment and wafer polishing processing. Polishing head holds wafers by vacuum and it rotates on the polishing pad. Slurry is delivered by slurry arm and polishing pad conditioner refreshes polishing pad surface as each wafer processing, which results in global planarization and polishing. Whereas, in microscale observation, complicated interaction among pad asperity-slurry (abrasive and chemistry)-wafer surface occurs during CMP processing, which is depicted in **Figure 3**. According to semiconductor process development, CMP process itself has developed its equipment, consumables, polishing functions and slurries to improve performance.

CMP performances are defined by removal rate (throughput), selectivity, planarization (planarity), within wafer non-uniformity, surface topography (roughness), corrosion and post CMP defects. The definitions of them are:

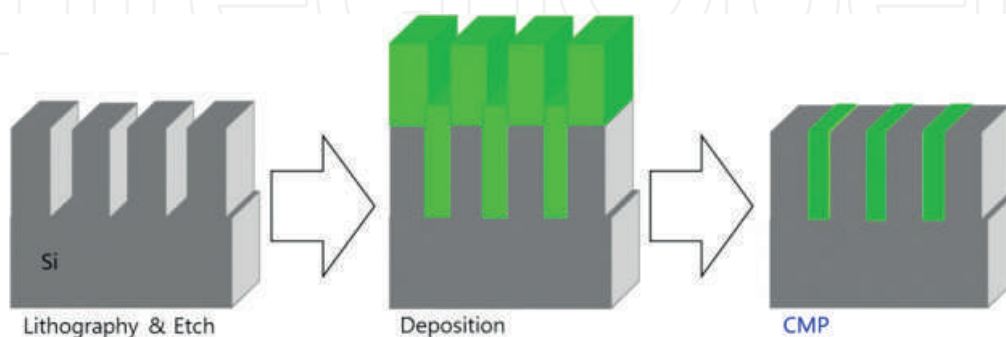


Figure 1. The concept of chemical mechanical polishing (CMP). Non-planarized topography becomes planarized surface by CMP.



Figure 2. The schematic mechanism of material removal by CMP.

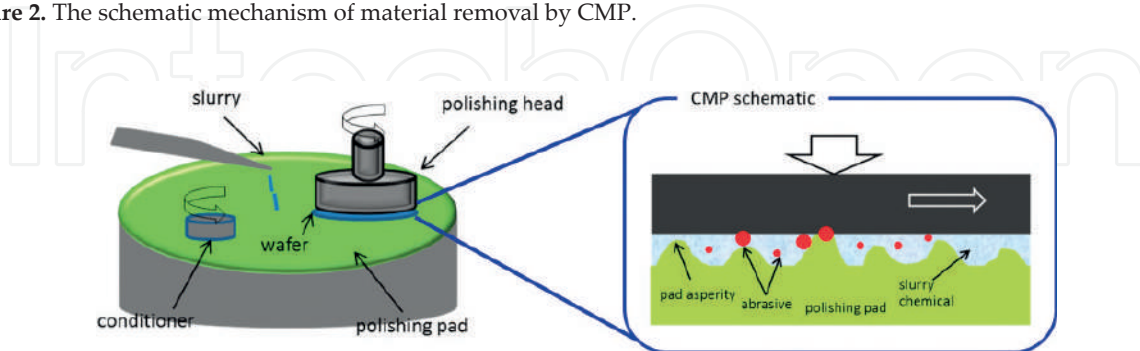


Figure 3. The schematic of conventional CMP equipment.

$$\text{Removal Rate (RR)} = (\text{pre CMP thickness} - \text{post CMP thickness}) / (\text{polishing time})$$

$$\text{Within Wafer Uniformity} = \text{Film thickness sigma post CMP} / \text{Film mean thickness post CMP}$$

$$\text{Selectivity (A:B)} = \text{RR of A material} / \text{RR of B material}$$

Planarization is commonly measured by step height reduction rate. These performances are closely related with device yield and electrical performances. For example, CMP-induced microscratch defect (**Figure 4**) is detrimental to device yield [3, 5]; transistor resistance is strongly influenced by post CMP uniformity, and residual material blocks subsequent patterning. CMP performances are determined by multiple CMP process factors; however, CMP slurry is the most influencing parameter. CMP slurry consists of abrasive particles and chemical components such as pH adjuster, dispersant, polymeric additives, oxidizer, and passivation agent, depending on polishing purpose to provide proper surface modification of material.

As described in **Figure 3**, direct contact between abrasive particle and wafer surface removes material, thus, properties and characteristics of abrasive particle and their understanding are inevitable to optimize CMP process. Although a lot of different kinds of abrasives have been tried for CMP applications, three abrasives have been employed successfully until recent device manufacturing. They are silica-based abrasive, ceria-based abrasive, and alumina-based abrasive. However, CMP is indispensable process for future semiconductor fabrication and it needs development of new abrasives for the success of new designed device and matured manufacturing. **Figure 5** shows CMP abrasive market trend in semiconductor industry [14]. Its growth expectation for the next 4 years is about 30% increase from 2016. This chapter introduces abrasive particles and their applications to CMP process for semiconductor manufacturing.

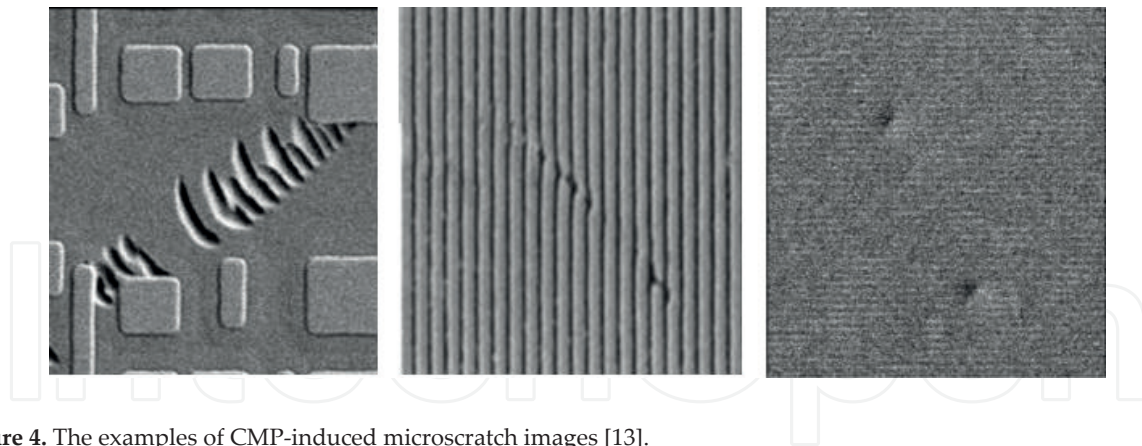


Figure 4. The examples of CMP-induced microscratch images [13].

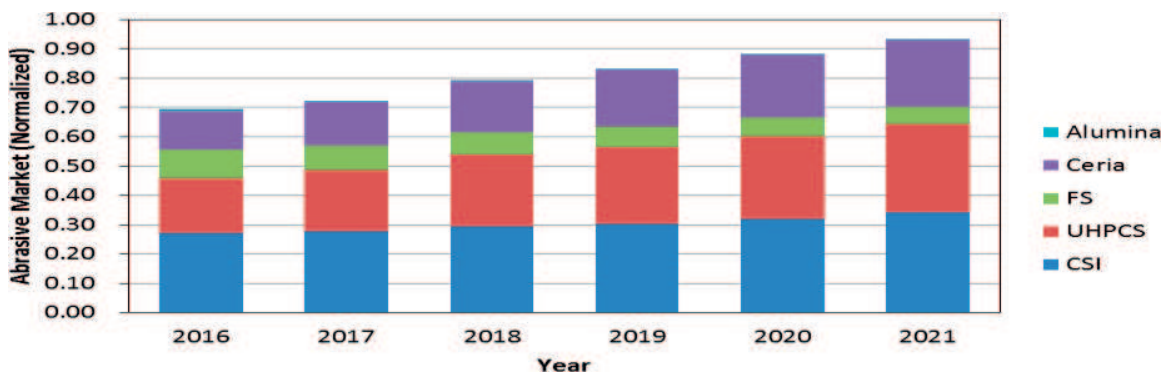


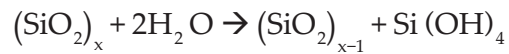
Figure 5. Slurry abrasive market trend (Reprinted from Ref. [14] with permission from author. Copyright Linx-consulting). FS is fumed silica, UHPCS is ultra-high purity colloidal silica and CSI is colloidal silica abrasive.

2. Abrasive for dielectric CMP

A dielectric material in semiconductor processing refers to insulating materials and mostly it indicates all kinds of silicon oxide materials [5]. Most dielectric CMP applications focus on transistor formation, which is called as front end of the line (FEOL) process. And dielectric CMP requires either oxide bulk CMP or CMP stop on 'stopper' material. For the stop on CMP case, oxide material is removed by CMP and CMP stops when stopper material is exposed. Shallow trench isolation (STI) CMP and interlayer dielectric (ILD) CMP are representative dielectric CMP applications. STI CMP process (stop on 'silicon nitride') is described in **Figure 6** [3] as an example of dielectric CMP. The stopper materials are mostly silicon nitride or polysilicon in FEOL process. For dielectric CMP purpose, two – three major abrasives are used in the advanced node semiconductor manufacturing.

2.1. Silica-based slurry and silica abrasive

As briefly described in the introduction, CMP mechanism is soft layer removal by abrasive particle. This section introduces silica particle as slurry abrasive. During dielectric CMP process, silicon oxide surface reacts with OH^- from the slurry solution and forms silicon hydroxide, $\text{Si}(\text{OH})_4$. The hydration reaction is.



And this soften $\text{Si}(\text{OH})_4$ is mechanically removed by silica abrasive [3, 15]. Then silicon oxide surface is exposed and hydration occurs again. This process is repeating until silicon oxide disappears. From **Figure 2**, soft layer can be considered as $\text{Si}(\text{OH})_4$ in this case. The hydration rate is influenced by the concentration of OH^- ions in the solution, thus alkaline environment can accelerate surface hydration and make fast material removal by fast reaction [2, 15–16]. Therefore high pH silica-abrasive slurry is favorable to obtain high removal rate. Two common synthesizing methods of silica abrasives are commercially used in the semiconductor industry. One is fumed process and the other is colloidal process [5, 17–19]. The typical abrasive images

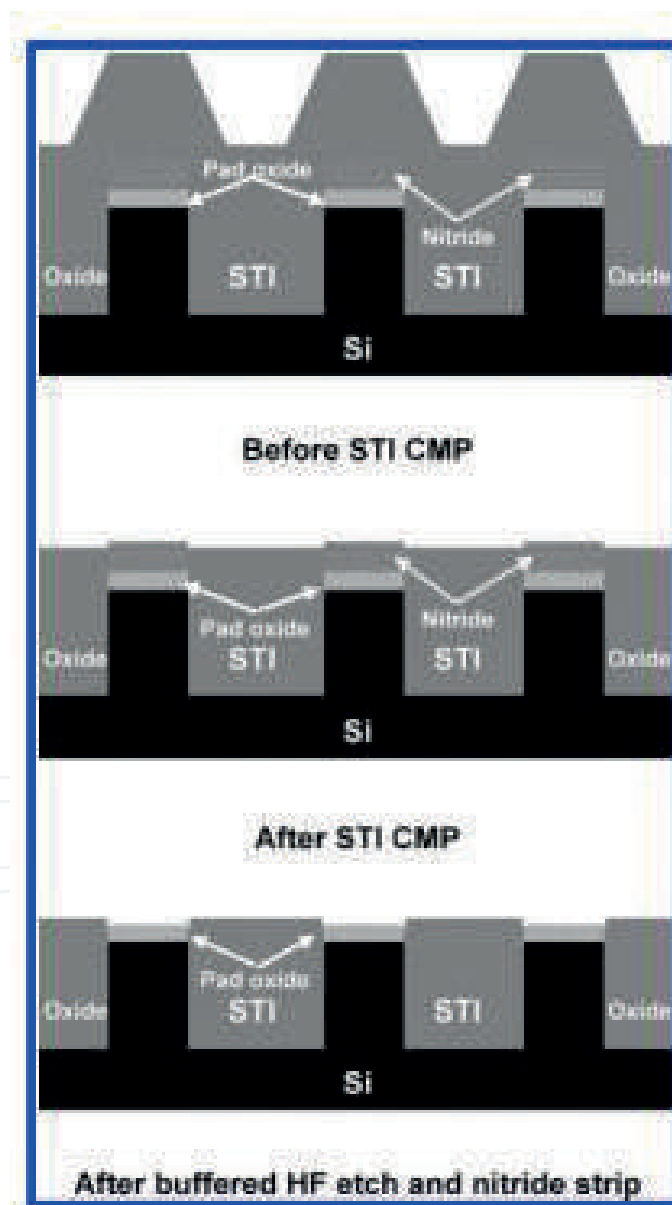
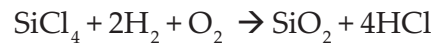


Figure 6. Procedure of shallow trench isolation (STI) CMP. Polishing stop on silicon nitride (Reprinted with permission from Ref. [3]. Copyright 2010 American Chemical Society).

of silica abrasive by each synthesis methods are shown in **Figure 7** [20, 21]. Fumed silica synthesis uses flame reaction of chlorosilane at high temperature, which is summarized at.



With this method, early development of silica abrasive particle size is larger than 300 Å, but development of filtration and post treatment enables to control the abrasive size below 150 Å. The commercial fumed silica abrasive slurry for dielectric CMP has high abrasive concentration to achieve enough removal rate. However, high abrasive concentration caused scratch defects, easy to agglomerate and clogging problem in slurry delivery system or filter.

Figure 8 shows example of clogged silica abrasive, which leads to significant defects on the wafer at post CMP. The whitish particles are silica abrasive in the slurry loop system. Therefore recent device manufacturing use high percentage of fumed silica abrasive slurry less and less, and forecast expects less usage of fumed silica abrasive as shown in **Figure 5**. Contrary to fumed method, colloidal abrasive is synthesized by liquid phase growth process via precursor [5, 16, 18–25]. Commonly, colloidal silica is made from sodium silicate (Na_2SiO_3) or sodium meta-silicate (NaHSiO_3). By ion exchange, sodium ion is eliminated and colloidal silica is formed to be used as CMP slurry abrasive. Colloidal silica abrasive slurry has much lower removal rate than fumed silica abrasive although it gives much lower scratch defect performance by its spherical shape and small size. To enhance removal rate of dielectric material by colloidal silica, organic cation is added as removal booster [16]. It changes colloidal silica abrasive surface charge from negative into positive and coulombic attraction force between abrasive and dielectric surface, which is negative, accelerates removal rate. As shown in **Figure 9(a)**, surface zeta potential behavior with respect to pH [26] can support this mechanism. Schematic of enhanced removal rate by colloidal silica abrasive is given in the same Figure. pH control is critical to this case. Recently, several attempts to new synthesis of silica abrasive to add

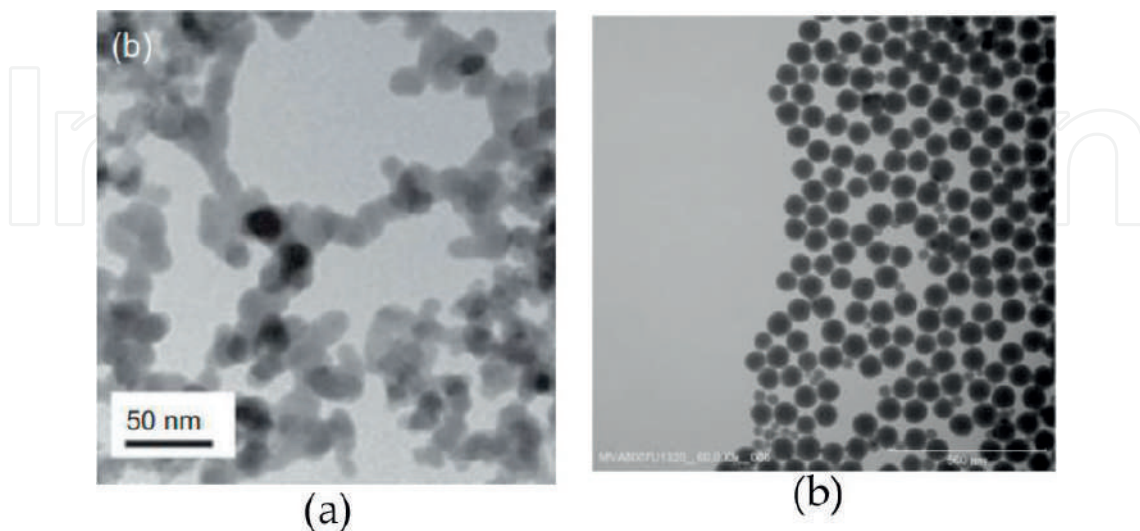
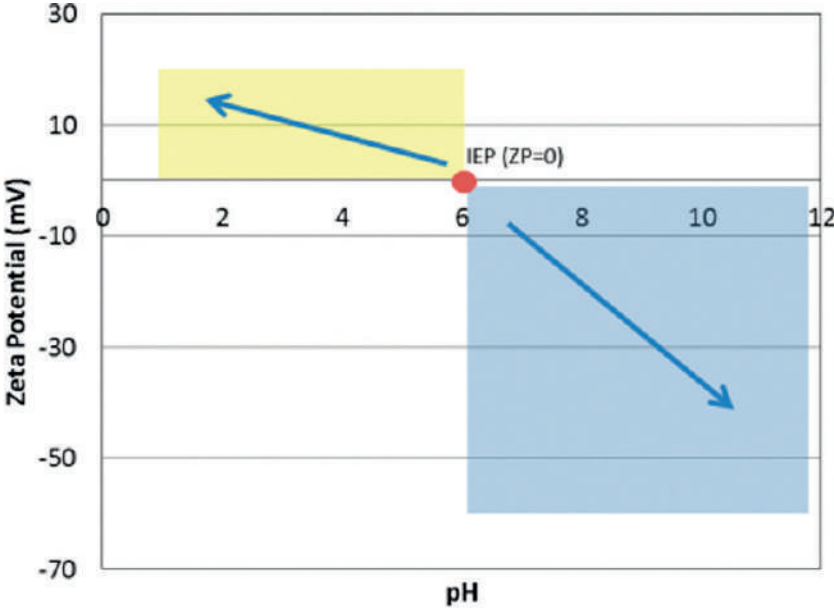


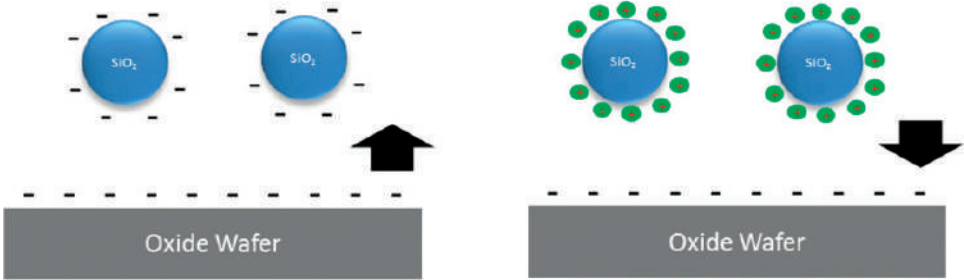
Figure 7. TEM images of (a) fumed (Reprinted by permission from [20], Copyright 2012 American Chemical Society) and (b) colloidal silica abrasive [21].



Figure 8. The clogged silica abrasive in slurry delivery loop.



(a)



(b)

Figure 9. (a) Zeta potential of SiO₂, and (b) silica abrasive without surface treatment and with surface treatment with organic cation at acidic region.

more stable particle distribution have been reported [26–29]. For instance, Pan et al. presented silane modified silica abrasive particle preparation to mitigate gelation of colloidal silica due to high chemically active hydroxyl group from silica surface. The siloxane groups in silane and hydroxyl groups in silica surface generate hydrolysis condensation reaction, which results in surface zeta potential change to improve dispersion stability [27].

2.2. Ceria abrasive for dielectric CMP slurry

Although high removal rate, low cost of ownership and effective planarization are obtained by silica abrasive, selectivity control and low scratch defect requirements bring ceria-based abrasive to be universally used in dielectric CMP of advanced node semiconductor manufacturing. And recent dielectric CMP uses ceria-based slurry much more than before (refers to **Figure 5**). The CMP mechanism by ceria-based slurry is different from silica-based slurry. Instead of mechanical removal by silica abrasive, ceria abrasive uses surface interaction with silicon oxide dominantly, which is.



Strong bonding between Ce and hydrated silicate detach silicon oxide and Si-O-Ce lump is removed from the surface [15, 30]. Ceria CMP process is shown in **Figure 10**.

Therefore, ceria abrasive surface charge control is important in determining CMP performance. The surface charge behavior can be indicated by ceria zeta potential property [31]. As shown in **Figure 11(a)**, isoelectric point (IEP) of ceria is \sim pH 8 (at acidic: positive charge, at alkaline: negative charge) and surface potential is opposite to silicon oxide at acidic environment. Thus, most ceria-abrasive slurry pH is less than 8 to facilitate Si-O-Ce formation. Similar to silica abrasive synthesis, two types of ceria-base abrasive are commonly synthesized for CMP applications [5, 31, 32]. They are calcined ceria abrasive and wet (or colloidal) ceria abrasive. Calcined synthesis is based on solid-state oxidation process. Raw ceria material is oxidized followed by mechanical crushing to make them small particles. And filtration removes large particles. Depending on crushing condition and filtration, calcined ceria abrasive size can be controlled. On the other hand, wet process uses precipitation procedure in liquid state. Seed ceria nuclei in an aqueous cerium solution grows and forms ceria (or cerium hydroxide) particles. Ceria abrasive made by wet process has spherical shape and narrow particle size distribution compared with calcined process. These synthesis methods and typical ceria abrasive images from each method are shown in **Figure 11(b)–(d)** schematically



Figure 10. The schematic mechanism of oxide removal rate by ceria abrasive.

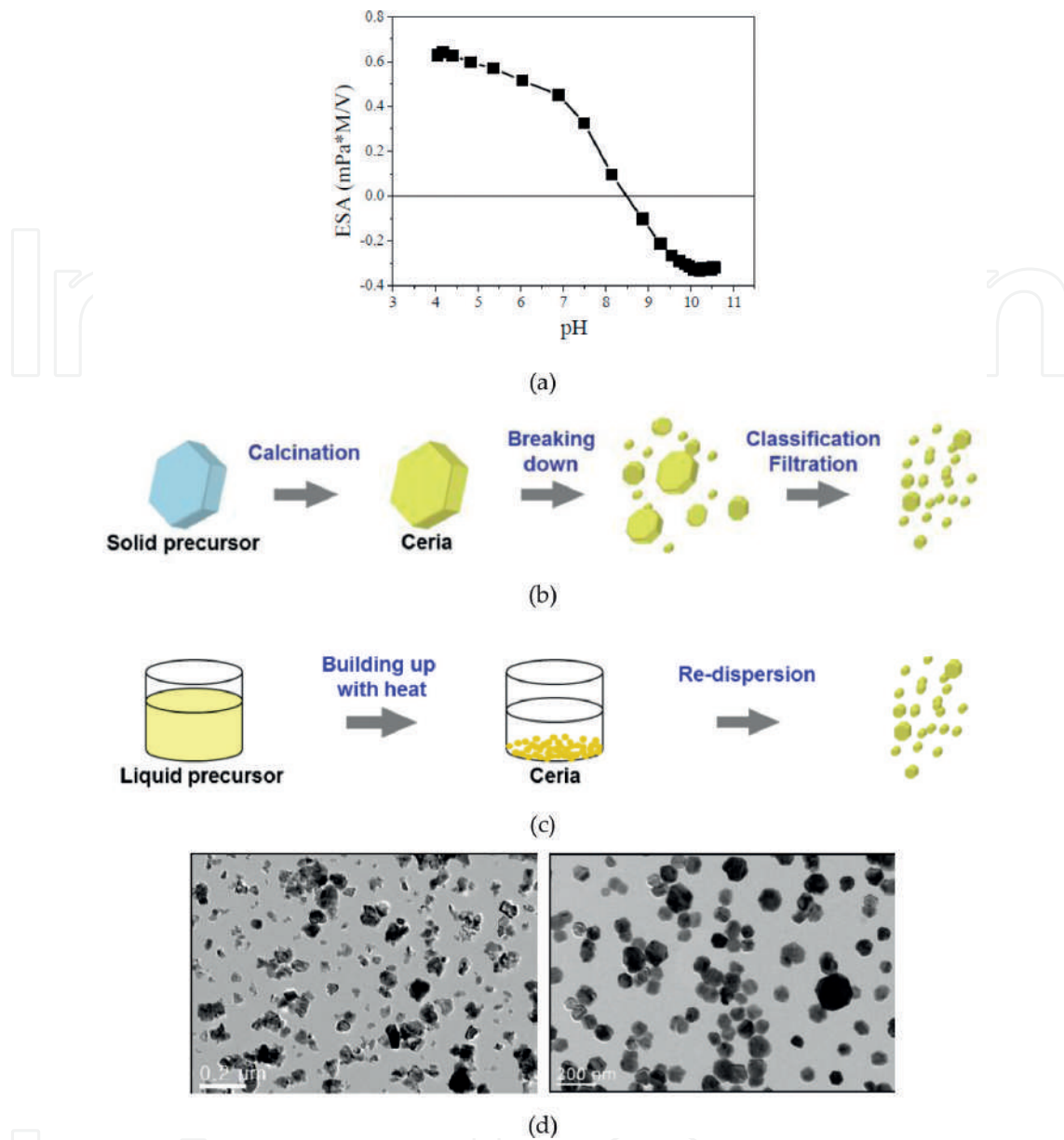


Figure 11. (a) Zeta potential curve of conventional ceria abrasive, (b) synthesis of calcined ceria abrasive, (c) synthesis of colloidal ceria abrasive, (d) TEM images of calcined (left) and colloidal (right) ceria abrasives ((a) & (d) reprinted by permission from mater. & interfaces, Jihoon Seo et al. [35], Copyright 2014 American Chemical Society) ((b)&(c) Reprinted from Ref. [34] with permission from authors)).

[31, 33–35]. The overall property comparison between calcined processed ceria abrasive and colloidal ceria abrasive is summarized in **Table 1** [31]. Calcined ceria abrasive slurry provides steady removal rate. Wet ceria abrasive slurry shows relatively lower removal rate than calcined ceria abrasive, however, the most critical advantage of wet ceria abrasive slurry is scratch defect improvement due to small and regular shape of abrasive particle. Recent study by Seo revealed Ce surface oxidation state had significant influence on the CeO₂ interaction to silicate and they investigated the effect of concentration of Ce³⁺ ions on the affinity to silicate ions and wet ceria particle size effect on the adsorption of silicate [35, 36]. Higher concentration of Ce³⁺ ions increased adsorption affinity with silicate ions and larger ceria abrasive has

Calcined CeO ₂	Colloidal CeO ₂
Mean particle size (nm): 150–500	Mean particle size (nm): 120–170
Relatively high oxide removal rate	Relatively low oxide removal rate
High crystallinity	Spherical shape
Tunable particle size	Uniform size distribution
Facet shape	High cost
Poor size distribution	Relatively low scratch
Mass production	
Relatively high scratch	

Table 1. Properties of calcined CeO₂ and colloidal CeO₂ (Reprinted from Ref. [31] with permission from author).

higher Ce³⁺ ions due to higher surface to volume ratio. In addition to calcined and wet process, flux method to synthesize ceria abrasive particle has proposed to overcome limitation of calcined or wet process [37]. It uses cerium nitrate hexahydrate (Ce(NO₃)₃·6H₂O) and potassium hydroxide (KOH) as starting material and ethylene glycol (C₂H₆O₂)-DI mixture as solvent. Through precipitation, hydrothermal reaction and centrifuging process, narrow size distribution with desirable characteristics ceria abrasives synthesis are demonstrated [37]. Ceria or ceria-based slurry application in CMP is increasing and advanced slurries with ceria abrasive are emerging in the semiconductor industry. Ultrafine (or nano-sized) ceria abrasive and composite abrasive will be introduced in Section 5.

3. Abrasive for tungsten CMP

Tungsten has been used for metal interconnection and contact formation. Many candidate metals have been developed to replace tungsten; however, tungsten is still standard metal for sub 14 nm contact formation due to its excellent electromigration and diffusion barrier performance [3, 38]. The CMP mechanism of tungsten was proposed by Kaufmann firstly [39]. A pristine tungsten surface is oxidized by oxidizer at acidic condition and it transforms to tungsten oxide (WO_x). The formation of oxide depends on solution and chemistry. Tungsten oxide plays a role as passivation layer to protect subsurface tungsten from dissolution or corrosion. And tungsten oxide is easy to be removed by mechanical force of abrasive since its hardness is less than pure tungsten. This process is repeated until CMP stops. Therefore, role of chemistry (in particular oxidizer) is important in tungsten CMP. Among many kinds of oxidizer, ferric nitrate (Fe(NO₃)₃-) is the most successful one [3, 5]. The schematic description of tungsten CMP mechanism is given in **Figure 12**. The common and commercially available slurry for tungsten CMP has alumina-base and silica-base abrasives [3, 5]. At sub 14 nm logic device fabrication, tungsten CMP is the most important process to enable transistor formation. It requires superior planarity and extremely accurate uniformity control. For this purpose, alumina abrasive showed better planarity and selectivity performance. Hence its utilization for bulk tungsten CMP is commonly adopted in advanced device manufacturing.

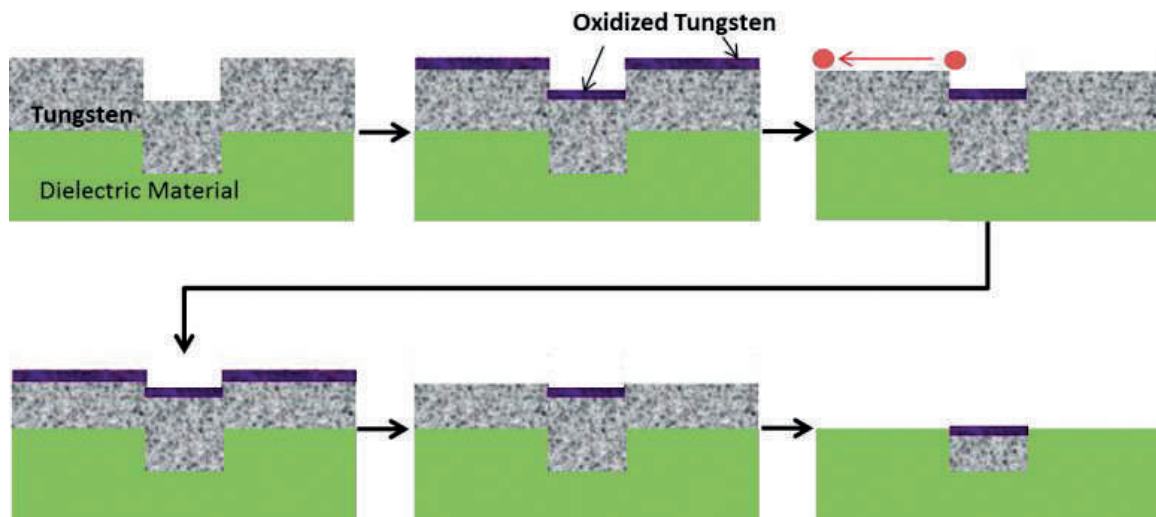


Figure 12. The mechanism of tungsten CMP.

Alumina abrasive has been synthesized by alum process and calcination [18]. For CMP application, alpha-alumina abrasive is commonly used. Hardness of alumina abrasive is much higher than tungsten and tungsten oxide, therefore it is easy to make scratch defect on the surface. Moreover, due to the surface charge difference between alumina and tungsten at acidic region, attractive force retains alumina abrasive on the wafer surface. Recently, composite alumina abrasive with polymeric material has been introduced in the industry due to defect concern at advanced node semiconductor [38]. Silica base slurry utilization on tungsten CMP is usually for non-selective CMP purpose (polishing both tungsten and dielectric material) because its selectivity with oxide is not as high as alumina abrasive slurry. Tungsten CMP is driven by chemical effect more than mechanical abrasion, removal rate strongly depends on chemical components (oxidizer, surfactant, and stabilizer) and activation condition (for example, process temperature) [39–41]. Therefore adequate combinations among them are essential to provide desired CMP performances. Although removal rate is linearly increasing with abrasive concentration in the slurry, loading effect (very low removal rate or non-linear removal rate behavior at the early stage of CMP) is more significant in tungsten CMP than dielectric CMP. Yttrium, ceria, zirconium and composite abrasives have been tried and under development for tungsten CMP applications [3].

4. Abrasive for copper CMP

Copper is introduced in semiconductor manufacturing for metal interconnection application mid-1990s and now it is standard metal for back end of the line interconnection [2–4, 10]. Accordingly, CMP for copper has been highlighted due to its process challenges. Like tungsten CMP, copper CMP mechanism is based on Kaufman’s model. Chemical reaction from slurry produces oxidized copper and abrasive particle removes oxidized copper. The major components of copper CMP slurry are abrasive, oxidizer, inhibitor, surfactant and chelating agent. The challenges of copper CMP are scratch defects and copper corrosion. Corrosion is

mostly induced by chemical in the slurry and most of scratch defects are driven by abrasive particle. In particular, hardness of copper is lower than most abrasive particles. Therefore, smaller size of abrasive with spherical shape and less abrasive content are favorable to the slurry formulation. The common copper CMP abrasives are alumina and colloidal silica [3, 10]. However, at advanced semiconductor manufacturing, colloidal silica abrasive becomes prevalent because it has appreciable polish rate of barrier material (tantalum/tantalum nitride). The copper removal rate and CMP performances are sensitively influenced by chemistries and components in slurry in conjunction with silica abrasive characteristics. Most of copper CMP slurry researches have focused on chemistry perspective instead of abrasives.

5. Advanced abrasives for future CMP applications

One of the most important requirements of CMP process in semiconductor application is scratch defect reduction, which has mentioned in this chapter several times. For abrasive perspective, smaller size abrasive particle is favorable for scratch defect. Therefore, recent abrasive technology has focused on nano-sized abrasive synthesis with minimized agglomeration. For dielectric CMP, nano-sized cerium hydroxide (or ultrafine cerium hydroxide or nano-ceria) abrasive slurry has been introduced due to its potential scratch defect reduction [33–34, 42–43]. The synthesis procedure of nano-sized cerium hydroxide abrasive is given in **Figure 13**.

Transmission electron microscope image of calcined ceria abrasive and nano-sized abrasive is compared in **Figure 14** [44]. Single abrasive size becomes as small as 5 nm. Even agglomerated abrasive size is less than 20 nm. Tanaka et al., showed removal rate and selectivity control by changing additives [33–34]. However, CMP mechanism of nano-sized cerium hydroxide abrasive is not clearly understood yet. Han et al. reported polishing pad surface roughness control is critical to maintain removal rate stability with nano-sized cerium hydroxide abrasive [44]. Kim proposed particle coverage model on the wafer as material removal mechanism with nano-sized cerium hydroxide abrasive [43]. In order to apply nano-sized cerium hydroxide abrasive for dielectric CMP, role of chemistry to enhance removal rate with selectivity control needs to be further explored.

Composite abrasive has drawn attention to the semiconductor industry recently. Each abrasive has its own unique properties. Some of them are very attractive and some of them are not good for desired CMP performances. Tries to combine advantages only from different abrasives have triggered ceria-silica composite abrasive development [45–48]. Researchers have paid attention to ceria-coated silica as next generation CMP slurry abrasive. Zhao et al.



Figure 13. Synthesis of nano-sized cerium hydroxide abrasive (reprinted from Ref. [33] with permission from authors).

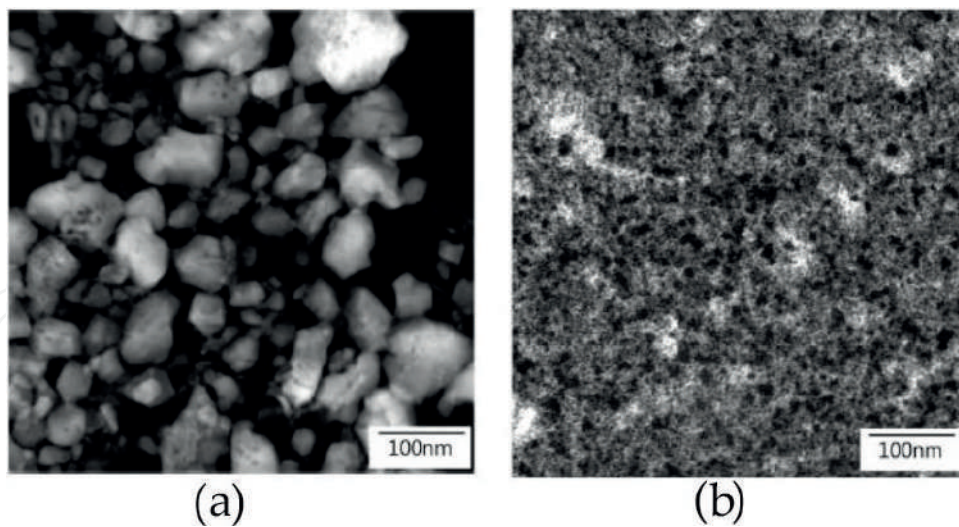


Figure 14. TEM images of (a) calcined ceria abrasive and (2) nano-sized cerium hydroxide abrasive (reprinted by permission from Ref. [44], Copyright 2013 Springer Nature).

uses sol-gel method to synthesize ceria-coated silica abrasive [48]. They prepared tetraethylorthosilicate and ammonia as raw materials, and composite nanoparticles are synthesized through precipitation procedure. About 150–200 nm spherical ceria-coated silica abrasives are successfully synthesized. Shell ceria size is 10 nm. Peedikakkandy et al. synthesized mono-dispersed ceria coated silica nanoparticles by micro-emulsion method and chemical precipitation process [46]. About ~10 nm crystalline ceria over silica with spherical shape and overall particle size <100 nm abrasive is successfully obtained. Zhang et al. synthesized ceria-coated silica abrasive by precipitation process using ammonium cerium nitrate and urea as precipitant with poly(vinylpyrrolidone) (PVP) as assistant [45]. With optimized synthesis conditions, <200 nm ceria-coated silica abrasive is obtained. In their study, X-ray diffraction confirms face centered cubic CeO_2 nanoparticle encapsulate core silica. Scanning electron microscope (SEM) shows uniformly distributed particles with spherical shape. Transmission electron microscope (TEM) directly shows evidence of homogenous nucleation of ceria particles and heterogeneous nucleation of silica particle with uniform, distinctive and crystalline ceria shell. With ceria-coated silica composite abrasive, higher removal rate than pure silica abrasive and comparable surface roughness is demonstrated on glass substrate CMP. Likewise ceria-coated ceria abrasive, Chen et al. reported composite abrasive containing solid silica core with silica mesoporous shell structure [29]. The advantage of mesoporous silica is its significant elastic recovery ability combined with ductile behavior. Chen et al. synthesized solid silica core via conventional Stöber procedure and shell silica encapsulating the core by means of modified Stöber process. It uses vinyltrimethoxysilane (VTMS) as silica source and cetyltrimethylammonium bromide as structure directing agent. Well defined spherical shape abrasives are successfully achieved and it shows clearly core-shell structure. The thickness of mesoporous silica shell is controlled by VTMS amount during synthesis. With this abrasive, higher removal rate of thermal silicon dioxide film and lower surface roughness are exhibited. Polymeric composite has drawn attention to CMP society due to its potential scratch defect reduction. Chen et al. reported polymer based core-shell abrasive aiming to reduce scratch

defect by CMP. The core abrasive is spherical polystyrene (PS) and ceria is selected as shell abrasive [49]. The mechanism of low scratch and minimize wafer damage is cushion effect of soft polymer core abrasive. In-situ chemical precipitation with mixture of deionized water, PS spheres, cerium nitrate hexahydrate ($\text{Ce}(\text{NO}_3)_3 \cdot 6\text{H}_2\text{O}$), and hexamethyleneteramine is used for this hybrid abrasive synthesis. As shown in **Figure 15**, it is clearly observed uniformly distributed ceria particles on the PS core, indicating the formation of core/shell structured abrasive particle. The ceria particle size is about 10 nm and face centered cubic structure which is confirmed by XRD and SAED pattern. Based on CMP test with thermal oxide film, PS/ceria hybrid abrasive slurry demonstrates lower removal rate, fewer scratches, and lower surface roughness are compared with ceria abrasive slurry.

Nano-sized ceria abrasive is already used in the semiconductor manufacturing. Ceria-silica or silica-silica composite abrasive is still under development stage although several unique synthesizes are suggested and demonstrate promising CMP data. Most of literatures with composite abrasive focus on material removal rate and surface quality. However, CMP application needs more performances. In order to be utilized in the industry, composite abrasives have to avoid agglomeration, need to robust abrasive stability, require optimized chemistry, and more CMP performances such as selectivity and defectivity must be fulfilled.

New materials CMP has emerged along with new device introduction and device node shrinkage, from ultra-soft materials such as porous low-k and photoresist to highly non-reactive metal such as ruthenium (Ru) [3–5, 50, 51]. Ultra-soft material CMP needs very soft abrasive or even abrasive-free slurry development [5]. Ru is little chemical reactive metal with high hardness. And it relies more on mechanical force to remove Ru layer than chemical dissolution. Moreover, RuO_4 , which can be produced by slurry chemistry, is toxic gas [50, 51]. Therefore Ru CMP has a lot of limitation to achieve enough removal rate by CMP. Cobalt (Co) is the most potential candidate metal for replacing tungsten as contact metal (or replacing Ta/TaN as barrier metal) and its CMP slurry abrasive development is upmost challenge for device fabrication [52–54]. Known issues by Co CMP are residual abrasive particle defects and Co corrosion. More difficulties on these materials are not only target material CMP but

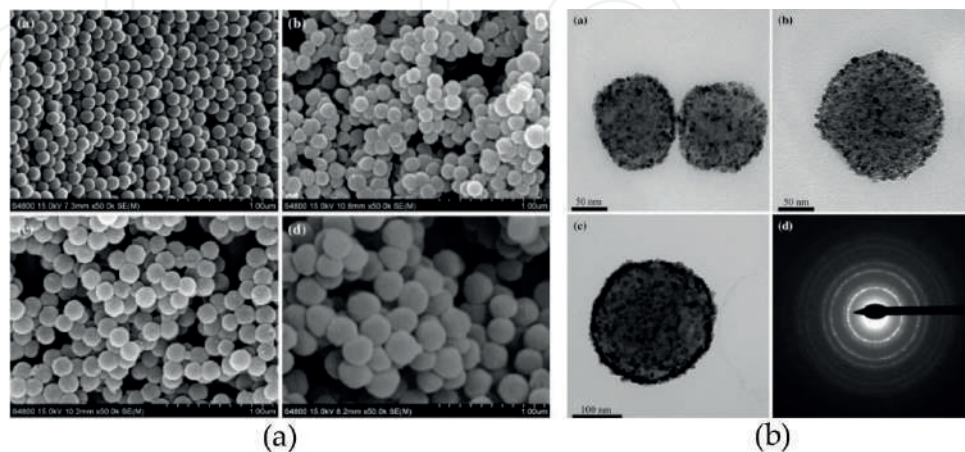


Figure 15. (a) SEM images and (b) TEM images of PS/ceria composite abrasive (Reprinted by permission from Ref. [49], Copyright 2016 Springer Nature).

also neighboring materials CMP for proper selectivity. Most of new materials CMP slurry is based on silica abrasive and chemistry optimization has been underscored. However, it still has a lot of opportunities to develop abrasives as well. Carbon based materials (either carbon nanotube or graphene) have drawn intense interests to the semiconductor industry for a long time. For CMP perspective, carbon-based material polishing, which has been rarely reported, is big challenge to abrasive development due to its high hardness.

6. Abrasive control in semiconductor fab

The role of abrasive in CMP application is to obtain enough material removal rate, desired selectivity and low defect (residual particle and scratch) performance. In addition to develop advanced abrasive material and synthesis, abrasive size distribution and dispersive ability in the solution has been developed to control large particle count. Particle size distribution is raw abrasive material nature resulting from synthesis, however, slurry distribution system and filtration can control large particles and agglomeration from the slurry without CMP performance degradation. In high volume semiconductor manufacturing fab, slurry distribution system is considered as infrastructure instead of equipment [18, 55]. It consists of (1) slurry drum, (2) agitation of drum (drum tumbling), (3) slurry blending and dispense, (4) daytank (or standby tank) with stirrer, (5) looping to tools. **Figure 16** shows simplified distribution system. Slurry is being circulated in the loop until it is used for CMP. Abrasive agglomeration is induced by shear stress, temperature change and chemistry variation if proper filtration is not implemented [56]. The location of filters from slurry distribution system is selected carefully. More filtration drops slurry flow pressure quickly by filter itself. Very fine filter will removes most abrasives, which results in low removal rate. Different slurry needs different type of filter and filtration at different locations; however global loop filtration and point of use (POU) filtration at polishing equipment are quite standard [18, 56, 57]. Global filter size is normally $>10\ \mu\text{m}$, which is bigger than POU filter to avoid flow pressure drop. POU filter size is smaller than $1\ \mu\text{m}$. Yi Wei et al., showed agglomeration behavior of different slurries.

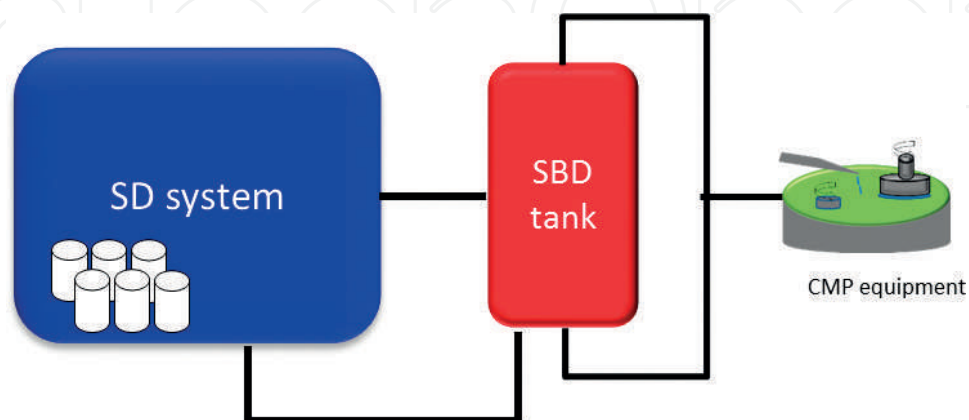


Figure 16. Slurry delivery facilities in semiconductor manufacturing fab. (SD = slurry dispense, SBD = standby distribution).

Colloidal silica abrasive agglomeration is more sensitive to shear stress than ceria abrasive. The most important challenge of filtration is plugging by abrasives. Three plugging mechanisms in filtration are well known, which are cake formation, gradual plugging, and complete plugging [58]. Cake formation is driven by particles build up on the filter surface, gradual plugging is induced by particles building up on the pore, and complete plugging indicates pore blocking by particles. Depending on particle size, deformability, and agglomeration, filtration procedure can be optimized. The most commonly used filter in CMP slurry is 'graded density depth' type. It has multi-layers of fibrous media and there is retention gradient along with flow direction. Commonly, large particles are captured first at outer layer and small particles are retained at inner layer. However, more advanced filter and filtration researches are reported recently. Nano-fiber based advanced filter to remove large abrasive as well as avoid agglomeration is reported. Morby et al., suggested composite/rigid structured filter which consists of thermally bonded polyolefin bi-component coarse fiber matrix and microfiber-glass web as next generation filter to retain slurry flow pressure and remove large abrasive effectively [59]. In addition to filtration, dispersant in the slurry prevents abrasive from agglomeration. For high abrasive content slurry case, abrasive particles are easy to sediment and agglomerate by particle charge interaction. Along with slurry abrasive development, advanced filter development and prevention of sediment of abrasive are required in slurry preparation.

7. Conclusion

This chapter reviews abrasives for CMP applications in semiconductor manufacturing. It includes abrasive types, abrasive synthesis, CMP mechanism and role of abrasives, and opportunities of new abrasive developments. Semiconductor business increases explosively and various semiconductor structures with high performance have been developed according to market requirement. In order to achieve mature semiconductor manufacturing, CMP process development is critical and abrasives in slurry play a pivotal role in determining CMP performances. The most common abrasive in dielectric CMP is either silica-based or ceria-based one. For metal CMP (tungsten and copper), silica is the most popular abrasive. Advanced synthesis for silica or ceria abrasives, new abrasive materials, and composite abrasives have studied for high performance CMP and new material CMP. Furthermore, the control of slurry abrasive in the looping is emphasized. Advanced filtration is critical to maintain abrasive size distribution. The applications of CMP are mostly focused on semiconductor industry; however its utilization expands to display industry, M/NEMs, automobile industry and biotechnology. The key of each application is noble abrasive development with proper chemistries.

Author details

Hong Jin Kim

Address all correspondence to: hongjin.kim@globalfoundries.com

Advanced Module Engineering, GLOBALFOUNDRIES, Malta, NY, USA

References

- [1] Li Y, edited. *Microelectronic Applications of Chemical Mechanical Planarization*. USA: John Wiley & Sons Inc; 2008
- [2] Steigerwald JM, SP Murarka, Gutmann RJ. *Chemical Mechanical Planarization of Microelectronic Materials*. USA: John Wiley & Sons Inc; 1997
- [3] Krishnan M et al. *Chemical Reviews*. 2010;**110**:178-204
- [4] Zantye PB, Kumar A, Sikder AK. *Materials Science and Engineering R: Reports*. 2004;**45**:89-220
- [5] Babu S. *Advances in chemical mechanical planarization (CMP)*. In: Woodhead Publishing Series in Electronic and Optical Materials. 2017
- [6] Tsujimura M. *Japanese Journal of Applied Physics*. 2016;**55**:06JA01
- [7] Hoffmann TY. *Solid State Technology*. 2010;**53**:20-23
- [8] Feeney P. *Solid State Technology*. 2010;**53**(10):14
- [9] Kim HJ et al. *Proceedings of Advanced Metallization Conference: 27th Asian Session 2017*. pp. 92-93
- [10] Ein-Eli Y, Starosvetsky D. *Electrochimica Acta*. 2007;**52**:1825-1838
- [11] Steigerwald JM. *Proceedings of IEDM*. 2008:37-40
- [12] Chi M-h. *Challenges in Manufacturing FinFET at 20nm node and beyond*. Technology Development, GlobalFoundries; 2014. http://www.rit.edu/kgcoe/eme/sites/default/files/Min-hwa%20Chi%20-%20abstract_%20Challenges%20in%20Manufacturing%20FinFET.pdf
- [13] Kim HJ. *International Conference on Planarization/CMP Technology*. AZ USA: Pheonix; 2010
- [14] <http://www.linx-consulting.com/>
- [15] Cook LM. *Journal of Non-Crystalline Solids*. 1990;**120**:152-171
- [16] White ML, Jones L, Romine R. *The mechanism of low pH silica based oxide slurries*. Cabot Microelectronics Technical Paper (<https://www.cabotcmp.com/cmp-research/cmp-technical-papers/>)
- [17] Tutorial, *Planarization Processes for ULSI Fabrication to the Year 2002 (SEMICON WEST, July 16, 1997)* p. 51
- [18] Li SH, Miller RO. *Chemical Mechanical Polishing in Silicon Processing*. USA: Academic Press; 2000
- [19] Doering R, Nishi Y. *Handbook of Semiconductor Manufacturing Technology*. 2nd ed. USA: CRC Press; 2008
- [20] Zhant H et al. *Journal of the American Chemical Society*. 2012;**134**(38):15790-15804

- [21] Gert Roebben et al. *Frontier in Chemistry*, Technical Report, Oct. 19, 2015 (https://www.researchgate.net/publication/283302479_Reference_materials_and_representative_test_materials_to_develop_nanoparticle_characterization_methods_The_NanoChOp_project_case)
- [22] Zhang KL et al. *Journal for Nanoscience and Nanotechnology*. 2009;**9**(2):1054-1057
- [23] Qin F, Liu W. *Proceedings of 2015 International Conference on Planarization/CMP Technology (ICPT)*. pp. 119-122
- [24] Kao MJ, Hsu FC, Peng DX. *Advances in Materials Science and Engineering*. 2014;**2014**:1-8
- [25] Ming-Shyong Tsai. *Materials Science and Engineering: B*. 15 January 2004;**106**(1):52-55
- [26] Park K-W et al. *Journal of the Korean Physical Society*. 2007;**51**(1):214-223
- [27] Shun G et al. *Wear*. 2011;**273**:100-104
- [28] Posthumus W et al. *Journal of Colloid and Interface Science*. 2004;**269**:109-116
- [29] Chen A et al. *Journal of Alloys and Compounds*. 2016;**663**:60-67
- [30] Hoshino T et al. *Journal of Non-Crystalline Solids*. 2001;**283**:129-136
- [31] Seo J. *Surface Chemistry of Ceria Nanoparticles for CMP Applications*. CAMP's 22th International Symposium on CMP; 2017
- [32] Raghavan S, Keswani M, Jia R. *Kona Powder and Particle Journal*. 2008;**26**:94
- [33] Tanaka T et al. *Proceedings of 2014 International Conference on Planarization/CMP Technology (ICPT)*. pp. 22-24
- [34] Minami H. *Polishing Selectivity Control for Scratch Free Nano Size Cerium Hydroxide Slurry*. CAMP's 19th International Symposium on CMP; 2014
- [35] Seo J et al. *ACS Applied Materials & Interfaces*. 2014;**6**:7388-7394
- [36] Seo J et al. *Applied Surface Science*. 2016;**389**:311-315
- [37] Myoung-Hwan O et al. *Powder Technology*. 2011;**206**:239-245
- [38] Broadbent EK et al. *IEEE Transactions on Electron Devices*. 1988;**35**:952-956
- [39] Kaufman FB et al. *Journal of the Electrochemical Society*. 1991;**138**(11):3460-3464
- [40] Kim HJ et al. *ECS Journal of Solid State Science and Technology*. 2014;**3**(10):P310-P314
- [41] Palla BJ et al. *IEEE/CPMT International Electronics Manufacturing Technology Symposium*. 1998. 155-163
- [42] Kim HJ, Qin L, Lee T. *TechConnect World Innov. Conf.* Washington DC, USA; 2015
- [43] Kim HJ, Lee TH, Ryan A. *ECS Transactions*. 2016;**72**(18):27-36
- [44] Han S et al. *Electronic Materials Letters*. 2013;**9**(2):155-159
- [45] Zhang Z et al. *Applied Surface Science*. 2010;**257**:1750-1755

- [46] Peedikakkandy L et al. Applied Surface Science. 2015;**357**:1306-1312
- [47] Chen G et al. Applied Surface Science. 2015;**359**:664-668
- [48] Zhao X et al. Microelectronic Engineering. 2010;**87**:1716-1720
- [49] Chen A et al. Journal of Materials Science: Materials in Electronics. 2016;**27**:2919-2925
- [50] Ruthenium CMP. Integration for Dual-Damascene Copper Interconnects. Cabot Microelectronics Technical Paper (<https://www.cabotcmp.com/cmp-research/cmp-technical-papers/>)
- [51] Cheng J et al. Proceedings of 2016 International Conference on Planarization/CMP Technology (ICPT). pp. 195-198
- [52] Alety SR et al. ECS Journal of Solid State Science and Technology. 2017;**6**(9):P671-P680
- [53] Changhong W et al. ECS Transactions. 2017;**77**(5):93-97
- [54] Turk MC et al. ECS Journal of Solid State Science and Technology. 2016;**5**(2):P88-P99
- [55] Mason M. CMP metrics improved by undiluted slurry data. Solid State Technology (<http://electroiq.com/blog/2011/06/cmp-metrics-improved-by-undiluted-cmp-slurry-data/>)
- [56] Lu Y et al. Proc. of 2014 International Conference on Planarization/CMP Technology (ICPT). pp. 291-295
- [57] Wu M et al. Proceedings of 2017 International Conference on Planarization/CMP Technology (ICPT), pp. 323-328
- [58] Yang HJ, et al. Semiconductor Technology International Conference (CSTIC), 2015. China: 2158-2297
- [59] Morby J, Entezarian M, Gieger B. Proceedings of 2015 International Conference on Planarization/CMP Technology (ICPT). pp. 128-131

IntechOpen

